SECURITY INFORMATION

Copy 278
RM E52J27

53-30-88
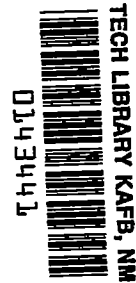
NACA RM E52J27

6781

RESEARCH MEMORANDUM

PRELIMINARY INVESTIGATION OF A PERFORATED AXIALLY

SYMMETRIC NOZZLE FOR VARYING NOZZLE

PRESSURE RATIOS

By Eli Reshotko

Lewis Flight Propulsion Laboratory
Cleveland, Ohio

RECEIPT SIGNATURE
REQUIRED

NATIONAL ADVISORY COMMITTEE
FOR AERONAUTICS
WASHINGTON
January 14, 1953

Classification cancelled (or changed to ...unclassified......)

By Authority of **NASA Tech PubAnnouncement**
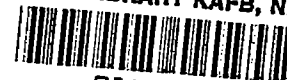(OFFICER AUTHORIZED TO CHANGE)
92 15 NOV 55

By.............. ...
....

....
GRADE OF OFFICER MAKING CHANGE)

...................lo Apr 6)......
DATE

1L   NACA RM E52J27   CONFIDENTIAL

2728

NATIONAL ADVISORY COMMITTEE FOR AERONAUTICS

RESEARCH MEMORANDUM

PRELIMINARY INVESTIGATION OF A PERFORATED AXIALLY SYMMETRIC

NOZZLE FOR VARYING NOZZLE PRESSURE RATIOS

By Eli Reshotko

SUMMARY

The performance characteristics of a perforated axially symmetric convergent-divergent nozzle were investigated in an attempt to achieve improved convergent-divergent nozzle thrust performance at below design pressure ratios. The purpose of the perforations was to allow inflow of air into the overexpanded portion of the nozzle, thus advancing separation of the flow.

The flow through the perforations was found to advance separation only when the perforations were liberally placed over the entire divergent portion of the nozzle. A local concentration of perforations caused separation only in the local region of perforation.

The use of low energy atmospheric bleed air reduced thrust losses by as much as 50 percent at appreciably overexpanded operation. For underexpanded flow, air flowing out through the perforations caused significant thrust loss. With shrouding to prevent this outbleed, thrusts 5 to 10 percent less than those of the unperforated nozzle were obtained. The use of high energy bleed was unsatisfactory since the inlet momentum penalty of the bleed air was in many cases greater than the additional thrust obtained.

INTRODUCTION

For operation at or above the design pressure ratio, the thrust ideally obtainable from a convergent-divergent nozzle is greater than the thrust obtainable from a convergent nozzle. Fixed-geometry convergent-divergent nozzles, however, have not generally been used for variable pressure ratio operation because of their poor thrust performance at below design pressure ratios. As an aid in the interpretation of the results of this investigation, the performance characteristics of a convergent-divergent nozzle will be reviewed.

Pressure

4

3

2

1

Design-point
chamber pressure

2728

Throat area   Exit
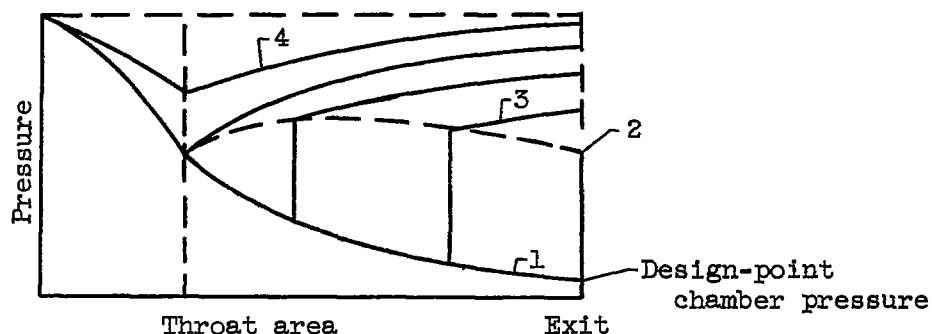
For operation at the design pressure ratio (curve 1), the pressure at the exit section of an ideal nozzle is exactly equal to the free-stream static pressure, which is herein assumed to be the static pressure of the region into which the nozzle is discharging. Underexpanded operation is obtained when the back pressure is lower than the design-point pressure so that additional free-jet expansion takes place outside the nozzle. The thrust obtained in underexpanded operation is less than could be obtained by isentropic expansion to the discharge pressure.

Overexpanded operation is obtained when the back pressure is higher than the design-point chamber pressure. With initial rise in back pressure, oblique shock formations will appear outside the exit section. These shocks will increase in strength until a normal shock is formed at the exit section (point 2). Thrust losses are realized in this type of operation since there are pressures on the divergent wall of the nozzle which are lower than the ambient pressure. With further increase in back pressure, the normal shock enters the nozzle and moves toward the throat (curve 3). After the normal shock reaches the throat, the nozzle "unchokes" thus allowing the throat pressure to increase as the back pressure is further increased (curve 4). Thrust losses are realized in this region of operation again because there are wall pressures in the divergent section that are lower than the back pressure.

The ideal variable nozzle is one which operates on design at all pressure ratios. For a fixed geometry nozzle, this would imply separation of the flow from the wall of the nozzle at the station where the static pressure of the jet stream is exactly equal to the back or free stream pressure. The present investigation was undertaken at the NACA Lewis laboratory in an attempt to obtain such a type of operation.

The purpose of this present investigation is therefore to determine whether flow bled through perforations introduced in the divergent portion of a convergent-divergent nozzle will improve the off-design

performance by causing the flow in the divergent portion of the nozzle to separate as described. Two types of bleed flow are considered. The first involves low stagnation energy bleed air (virtually at rest with respect to the nozzle) at ambient pressure applied to the perforations; the second involves bleed at prescribed pressures to simulate the effect of using some source of high pressure air. The case of the perforated nozzle with zero bleed flow is also considered.

In addition to the tests indicated, an unperforated convergent-divergent nozzle and a convergnet nozzle were tested for purposes of comparison.

The tests herein reported are for discharge into quiescent air. The effects of variation of size, shape, and configuration of the perforations were not considered.

DESCRIPTION OF APPARATUS AND METHOD

The basic nozzle used in this investigation is an axially symmetric nozzle designed by the method of characteristics for an exit Mach number of 2.186. The coordinates of this nozzle were corrected for turbulent boundary-layer displacement thickness by application of the method of reference 1 and are given in table I. A sketch of the basic nozzle is shown in figure 1. The nozzle was used in three forms: (a) perforated convergent-divergent, (b) unperforated convergent-divergent, and (c) convergent. These are shown in figure 2. (The symbols used throughout this report are defined in appendix A.) The nozzle was instrumented with wall static-pressure taps as indicated in table II.

In the tests to determine wall static-pressure distributions, the nozzles (unperforated convergent-divergent and perforated convergent-divergent) were mounted as shown in figure 3, drawing air in from the room. For zero bleed, a solid plate A was used. For ambient bleed, holes were drilled in this plate to allow the ambient discharge pressure to be applied to the perforations.

In the tests to determine jet thrust of the various nozzles, the nozzles were mounted in the apparatus shown in figure 4. The supply air to this apparatus was at a dew point of approximately -20° F. The wall pressure distributions presented, except those of figures 5 to 7, were obtained with the nozzle mounted in the apparatus of figure 4.

In the apparatus of figure 3, varying nozzle pressure ratios were provided by varying the pressure in the exhauster line. The inlet total pressure was relatively constant at atmospheric pressure. For each setting of exhaust line pressure, readings were taken of the wall static taps. The perforation procedure in these tests consisted of drilling

holes at various stations and determining the effect on the wall pressures. All perforations were 1/8 inch in diameter. The first perforations were at stations near the exit of the nozzle. A test was also run to determine the effect of a concentration of perforations at a station near the throat.

In the apparatus of figure 4, pressure ratio was established by setting both the upstream primary total pressure and the pressure in the exhauster chamber. For the low pressure ratios, the upstream primary total pressure was kept at approximately one atmosphere and the exhauster chamber pressure was varied. For high pressure ratios, the exhauster chamber pressure was held at about 3 inches of mercury absolute and the upstream primary total pressure was varied. The maximum pressure ratio attainable was about 21. Secondary or bleed air was tapped off the primary flow line upstream of the primary weight-flow measuring orifice. By means of suitable valves, it was throttled down to the desired secondary pressures.

Wall pressures were read on a mercury manometer board to the nearest 0.05 inch. The calibration of the thrust cell in the apparatus of figure 4 was checked before every run.

DISCUSSION OF RESULTS

In determining and evaluating nozzle performance, it is useful to record both the wall static pressures and the force thrust of the nozzle. Examination of the wall static-pressure profiles gives some insight into the characteristics of the internal flow whereas the force testing indicates over-all nozzle performance. The thrust of the nozzle may also be calculated by integration of wall pressures. This value, however, is expected to exceed the thrust force measurement by the amount of the internal friction drag.

Wall Static-Pressure Distributions

Unperforated convergent-divergent nozzle. - The wall static-pressure data for the unperforated convergent-divergent nozzle are presented in figure 5. The dashed lines in this figure indicate the calculated wall pressures for one-dimensional flow in the same nozzle. The actual wall pressure data for off-design pressure ratios do not conform at all to the values calculated from one-dimensional theory because of the inability of one-dimensional theory to predict the effect of the interaction between the shock waves and the boundary layer when the nozzle is overexpanded. According to one-dimensional theory, the normal shock at the exit section of the nozzle will not begin to move upstream in the nozzle until the back pressure exceeds 0.52 of the nozzle inlet total

2728

pressure (or unless the nozzle pressure ratio drops below 1.9). Experimentally, it was observed that the shock had already begun moving upstream at a nozzle pressure ratio of 3.60. It is interesting to note that reference 2 allows the prediction of the maximum back pressure (or minimum nozzle pressure ratio) for which there may be a normal shock at the exit of the nozzle. This point is indicated in figure 5. In all probability, the shock entered the nozzle before this maximum back pressure was exceeded. As a further indication of the nonconformance to one-dimensional theory, when the nozzle was operated at a pressure ratio of 1.55, the shock occurred at an area ratio of about 1.18 rather than at the predicted value of 1.65.

Since the actual wall pressures were higher than predicted, the obtainable thrusts are also higher. This point is brought out in reference 3. The difference between the actual curve for complete expansion and the one-dimensional curve may be due to condensation effects in the nozzle and possibly to excessive boundary-layer displacement thickness.

Perforated convergent-divergent nozzles - ambient bleed. - With the introduction of perforations near the exit section of the nozzle, effects were noticed which seemed to be dependent on the number of perforations introduced. For the condition of least perforation shown in figure 6(a), there is a slight increase in wall pressures near the exit of the nozzle but it is not sufficient to indicate separation. With the introduction of more perforations near the exit, the wall pressures decreased to the extent that they became noticeably less than the wall pressures for the unperforated nozzle. The tendency toward separation was therefore reduced, and the upstream movement of the shock in the nozzle was retarded. A comparison of the curves of figures 6(a) and 6(b) indicates, however, that for the same perforation configuration there was a more advanced tendency toward separation with decrease in nozzle pressure ratio (rising back pressure). The configuration that gave the poorest performance at a nozzle pressure ratio of 3 was improved at a pressure ratio of 2.2 to the extent that the wall pressures were about equal to those for the unperforated nozzle. This was probably an effect of the increased back pressure and consequently greater mass flow through the perforations at higher velocities. The wall pressure distribution for the completely perforated nozzle with ambient bleed is presented in figure 6 for comparison. These pressures were generally higher over most of the length of the nozzle because of the cumulative effect of bleed throughout the divergent portion of the nozzle. Figure 6(a) shows that in the region of the throat $(A/A_t = 1.0)$, wall pressures are lower for the completely perforated nozzle than for the unperforated nozzle. This occurs because of outbleed through these perforations since the throat pressure is greater than ambient pressure.

A concentration of perforations in the vicinity of the throat seemed to cause local separation in the region of the perforations

(fig. 7). The flow reattached for nozzle pressure ratios greater than about 1.60, however.

The completely perforated nozzle had highest wall pressures over most of the operating range. The wall pressures for this nozzle with ambient bleed are shown in figure 8. The pressure distributions appear to indicate some separation at almost all pressure ratios.

In an attempt to reobtain unperforated nozzle performance, the completely perforated nozzle was shrouded so as to eliminate net bleed. The outbleed near the throat of the nozzle reentered further downstream. The resulting wall pressure distributions are shown in figure 9. The wall pressure distributions are somewhat different from those of figure 5. Whereas in figure 5 there was no separation indicated before the shock occurred in the divergent portion of the nozzle, it appears that the additional roughness of the drilled holes caused some separation of the flow upstream of the shock. Also, the wall pressure distribution for complete expansion of the nozzle of figure 9 is lower than that of the unperforated convergent-divergent nozzle (fig. 5), indicating a thrust penalty imposed by bleed holes even without bleed flow.

Perforated convergent-divergent nozzles - pressurized bleed. - The bleed cases so far presented are for ambient bleed. Figures 10(a) and 10(b) present wall static-pressure distributions for bleed pressure equal to 0.4 of inlet total pressure and for bleed pressure equal to inlet total pressure, respectively. In figure 10(a) $(P_s/P_p \approx 0.4)$ the pressure distributions at low area ratios do not change appreciably with pressure ratio, whereas for area ratios greater than 1.3 the rate of pressure rise depends definitely on the operating pressure ratio. The wall pressures here are fairly high, especially for the large pressure ratios. The shapes of the pressure distributions shown in figure 10(b) are quite different from those of figure 10(a). The pressure decreases steadily down the nozzle to the exit pressures. The large influx of bleed weight flow also seems to prevent the throat from becoming choked.

Nozzle Thrust Data

The jet thrust data for the nozzles tested in this investigation are presented in the form of thrust coefficients. Jet thrust is a function of only the nozzle pressure ratio and does not depend directly on the flight conditions. The net thrust of a nozzle is obtained by subtracting the momentum of the incoming flow from the jet thrust. The net thrust will be further considered in the discussions involving incremental thrust ratio. The jet thrust parameter F_j/δ_t for the ideal nozzle, the actual nozzle, and the ideal convergent nozzle are defined in appendix B. In figure 11, F_j/δ_t as a function of pressure ratio is plotted for the ideal nozzle and the ideal convergent nozzle. The jet

thrust coefficient C_j is defined in appendix B as the ratio of the actual jet thrust of the nozzle to the jet thrust of the ideal nozzle at the same operating pressure ratio.

As shown in figure 12, the convergent nozzle had highest jet thrust coefficients of any of the nozzles presented for pressure ratios less than 5. It is also to be noted that for pressure ratios less than 2.5, the perforated convergent-divergent nozzle had thrust coefficients which were about midway between those of the unperforated convergent-divergent nozzle and the convergent nozzle. However, even at the higher pressure ratios, the thrust coefficients of the perforated nozzle never signifi-cantly exceeded those of the convergent nozzle. The thrust coefficients for the shrouded perforated nozzle with no bleed were generally somewhat lower than those of the unperforated convergent-divergent nozzle, but showed the same trends with pressure ratio.

The thrust coefficients for the nozzles with bleed were calculated in two ways. The first of these was on a constant total weight flow basis. The sum of the primary weight flow and the weight flow through the perforations was assumed constant and equal to the primary weight flow of the unperforated convergent-divergent nozzle. This condition implies a smaller throat for the perforated nozzle than for the unperfo-rated nozzle. On this basis it is noted (fig. 13(a)) that for $P_s/P_p > 0.6$, slightly higher thrusts were obtained for the bleed cases than for the unperforated nozzles for pressure ratios of about 2.5 or less. On a constant primary throat area basis (fig. 13(b)), thrust coefficients were obtained which in each case were greater than those of the shrouded perforated nozzle with no bleed. It is also to be noted that the jet thrust coefficients can exceed unity since additional weight flow is taken in through the perforations. The curves for $P_s/P_p = 0.8$ and $P_s/P_p = 1.0$ did not differ greatly possibly because the total weight flow (sum of primary and bleed weight flows) for these two bleed pressures was about the same.

Weight Flow Data

Weight flow information for all but the cases of pressurized bleed is presented in figure 14 in terms of the corrected weight flow parameter $W_p\sqrt{\theta}/A_t\delta_w$ and flow coefficient C_D. The flow coefficient C_D is defined as the ratio of measured weight flow to the weight flow of a choked ideal nozzle having the same throat area. For choked flow, the flow coefficient for all nozzles averaged 0.98. The convergent-divergent nozzles (without bleed) remained choked throughout the test range whereas the perforated nozzle and the convergent nozzle were unchoked at a pres-sure ratio of about 1.5.

2728

For the cases of pressurized bleed (fig. 15) the primary throat was choked over the entire range for $P_s/P_p < 0.6$. The throat, however, unchoked for $P_s/P_p = 0.8$; the maximum flow coefficient for this case was 0.91. The maximum flow coefficient for $P_s/P_p = 1.0$ was 0.79. The corrected ratio of bleed weight flow to primary weight flow is plotted in figure 16. The ratio remains constant for pressure ratios above which there is no change in internal wall pressure distribution.

Incremental Thrust Ratio - Turbojet and Ram-Jet Assumptions

To properly evaluate the thrust characteristics of various exit configurations, especially those involving weight flows in addition to the primary weight flow, the exit nozzles may be considered as part of a complete propulsive system. The net internal thrust of the system is thus a function of the flight conditions so that certain flight plan assumptions must be made to carry out this calculation. The expressions for net thrust (thrust with inlet momentum subtracted) for the ideal nozzle and ideal convergent nozzle are derived in appendix C. The flight plan assumptions for turbojet and ram-jet systems are given in appendix D.

Since the convergent nozzle is in most widespread use at present, its performance serves as a reference value in the expression for incremental thrust ratio. Incremental thrust ratio is defined as $(F-F_c)/F_{c_i}$. All quantities in this expression are net thrusts. This expression can be modified somewhat in the numerator. For cases of no bleed and equal inlet momentum,

$$F - F_c = \delta_t \left[\left(\frac{F_j}{\delta_t} \right) - \left(\frac{F_j}{\delta_t} \right)_c \right]$$

For cases with bleed,

$$F - F_c = \left\{ \delta_t \left[\left(\frac{F_j}{\delta_t} \right) - \left(\frac{F_j}{\delta_t} \right)_c \right] - (\text{bleed inlet momentum}) \right\}$$

The relations for incremental thrust ratio for both pressure and force data are presented in appendix D. The variation of incremental thrust ratio with flight Mach number for the turbojet and ram-jet assumptions is presented in figures 17 and 18, respectively.

The differences in magnitude between the thrust calculated from wall pressure integration and force data would be caused primarily by internal friction along the walls of the nozzle. For the unshrouded perforated nozzle with ambient bleed the difference is especially large

at high pressure ratio operation (figs. 17 or 18). This indicates probable loss of weight flow through the bleed holes.

In addition to the curves whose trends were already indicated in figure 12, a curve was drawn (figs. 17(b) and 18(b)) showing the performance of the perforated nozzle taking bleed air from the free stream through a normal shock diffuser. For the turbojet (fig. 17(b)), this curve follows that of the nozzle with ambient bleed (no bleed inlet momentum) very closely. For the ram jet (fig. 18(b)), however, it is readily noted that the performance of this configuration is the poorest of any shown. The thrust realized from the bleed weight flow was generally insufficient to balance the inlet momentum penalty involved in its induction.

For the turbojet (fig. 17(b)) the convergent nozzle gives highest thrust to $M_0 = 1.4$, with the unperforated convergent-divergent nozzle giving highest thrust for $M_0 > 1.4$. The perforated nozzle gives about 15 percent less thrust than the convergent nozzle for $M_0 < 0.9$ and about 5 percent less thrust between $M_0 = 1.2$ and $M_0 = 1.45$. At this point it would be advantageous to shroud the perforations and thus eliminate bleed rather than to continue with ambient bleed at the perforations. The resulting shrouded nozzle gives 5 percent to 10 percent less thrust than the unperforated nozzle as flight Mach number is increased from 1.45 to 2.8.

The case of zero bleed inlet momentum in all probability is unattainable. However, the curves for bleed cases are probably somewhere between the curve of zero bleed momentum and the curve for full bleed inlet momentum. The break in all the curves at $M = 0.9$ for the case of the turbojet occurs because of an abrupt change of altitude in the assumed flight plan (appendix D).

The curves for ram-jet performance with the same nozzles (fig. 18) are the same except for the Mach number range. It is here seen (fig. 18(b)) that the convergent nozzle suffices to a Mach number of 2.

CONCLUDING REMARKS

The perforated nozzle did not perform as expected. In the region of overexpanded flow, separation did not take place at the desired station for a given pressure ratio, while for high nozzle pressure ratios, loss of weight flow through the perforations caused significant thrust losses. The perforated nozzle might find application where bleed air is available internally (e. g., from boundary-layer bleed). The air can be put through the perforations rather than be ejected to the free stream.

This may be of some advantage in the overexpanded region. However, it must be ascertained that there is sufficient bleed flow since an insufficient amount may be worse than no bleed at all. Where the nozzle would ordinarily be underexpanded, the perforations can be closed off by a shroud.

It is felt that the use of larger divergence angles in the divergent portion of the nozzle would facilitate separation and therefore result in better nozzle performance at overexpanded conditions.

SUMMARY OF RESULTS

The following results were obtained from an investigation of the flow characteristics and thrust performance of a perforated axially-symmetric convergent-divergent nozzle:

1. The flow through the perforations was found to advance separation only when the perforations were liberally placed over the entire divergent portion of the nozzle. A local concentration of perforations caused separation only in the local region of perforation.

2. The convergent nozzle gave the greatest thrust of all the nozzles tested for pressure ratios less than 5. The unperforated convergent-divergent nozzle gave greatest thrust for pressure ratios greater than 5.

3. Use of low energy bleed air (no inlet momentum penalty) through perforations reduced thrust losses by as much as 50 percent at appreciably overexpanded operation. With high energy bleed air, the bleed system drag exceeded the reduction in thrust losses due to the bleed. For design point or slightly overexpanded operation, the presence of perforations was undesirable because of the loss of mass flow through the open perforations. Even with the perforations closed off externally, the remaining internal roughness caused 5 to 10 percent reduction in thrust from that of the unperforated convergent-divergent nozzle.

Lewis Flight Propulsion Laboratory
        National Advisory Committee for Aeronautics
                Cleveland, Ohio

APPENDIX A

SYMBOLS

The following symbols are used in this report:

A $\quad$ area perpendicular to nozzle axis

A_s $\quad$ area of external scoop

C_D $\quad$ flow coefficient, ratio of measured weight flow to the weight flow
$\quad\quad$ of choked ideal nozzle having same throat area

C_j $\quad$ jet thrust coefficient, $\left(\dfrac{F_j}{\delta_t}\right)\Big/\left(\dfrac{F_j}{\delta_t}\right)_i$

C_v $\quad$ velocity coefficient, ratio of actual exit velocity to exit veloc-
$\quad\quad$ ity of ideal nozzle at same pressure ratio

F $\quad$ net thrust

F_j $\quad$ jet thrust

M $\quad$ Mach number

P $\quad$ total pressure

p $\quad$ static pressure

r_e $\quad$ ratio of turbine exit total pressure to compressor entrance total
$\quad\quad$ pressure for turbojet engine; ratio of total pressure at exit of
$\quad\quad$ combustion chamber to total pressure at entrance to combustion
$\quad\quad$ chamber for ram-jet engine

r_i $\quad$ pressure recovery of inlet

T $\quad$ total temperature

t $\quad$ static temperature

W $\quad$ weight flow

α $\quad$ orientation angle of wall static-pressure taps to main line of taps

γ $\quad$ ratio of specific heats

δ_t $\quad$ ratio of static pressure at flight altitude to sea-level static
$\quad\quad$ pressure of NACA standard atmosphere

δ_w ratio of total pressure at nozzle entrance to sea-level pressure
        of NACA standard atmosphere

θ ratio of total absolute temperature at nozzle inlet to absolute
        temperature of NACA standard atmosphere at sea level

Station subscripts:

0   free stream or ambient

e   exit section of nozzle

p   main flow through nozzle (primary)

s   bleed or bleed chamber (secondary)

t   throat

w   wall

Other subscripts:

a   actual

c   convergent nozzle

i   ideal

sl   NACA standard atmosphere sea-level conditions

APPENDIX B

METHOD OF CALCULATION OF NOZZLE JET THRUST AND

JET THRUST COEFFICIENT

General nozzle jet thrust. - From momentum considerations at the nozzle exit section, the jet thrust force can be written

$$F_j = p_e A_e (1 + \gamma M_e^2) - p_0 A_e \tag{B1}$$

also,

$$\delta_t = \frac{p_0}{p_{sl}}$$

and therefore,

$$\frac{F_j}{\delta_t} = P_{sl} A_e \left[\frac{p_e}{p_0} (1 + \gamma M_e^2) - 1 \right] \tag{B2}$$

Ideal nozzle. - The ideal nozzle is defined as that expanding the flow to ambient pressure at all pressure ratios $(p_e = p_0)$. Substituting the relation $p_e = p_0$ in equation (B2) gives

$$\left(\frac{F_j}{\delta_t} \right)_i = P_{sl} A_e \gamma M_e^2 \tag{B3}$$

Evaluating A_e/A_t and M_e in terms of P_p/p_0 and substituting in equation (B3) give

$$\left(\frac{F_j}{\delta_t} \right)_i = P_{sl} A_t \gamma \sqrt{\frac{2}{\gamma-1}} \left(\frac{2}{\gamma+1} \right)^{\frac{\gamma+1}{2(\gamma-1)}} \left(\frac{P_p}{p_0} \right) \sqrt{1 - \left(\frac{P_p}{p_0} \right)^{\frac{1-\gamma}{\gamma}}} \tag{B3a}$$

Actual nozzle. - Actual nozzle performance is given on a coefficient basis:

$$\left(\frac{F_j}{\delta_t} \right)_a = C_j \left(\frac{F_j}{\delta_t} \right)_i \tag{B4}$$

where $C_j = C_D \times C_V$, the product of the flow coefficient and velocity coefficient.

Ideal convergent nozzle (choked). - The ideal convergent nozzle has sonic flow at the exit section when the flow is choked. For unchoked flow, the ideal nozzle relation (equation (B3a)) can be used. For a choked exit section,

$$p_e = \left(\frac{2}{\gamma+1}\right)^{\frac{\gamma}{\gamma-1}} P_p \quad \text{and} \quad A_e = A_t$$

Substituting in equation (B2) results in

$$\left(\frac{F_j}{\delta_t}\right)_{c_i} = P_{sl}A_t \left[(1 + \gamma)\left(\frac{2}{\gamma+1}\right)^{\frac{\gamma}{\gamma-1}}\left(\frac{P_p}{P_0}\right) - 1\right] \tag{B5}$$

2728

APPENDIX C

NET THRUST CONSIDERATIONS

<u>General.</u> -
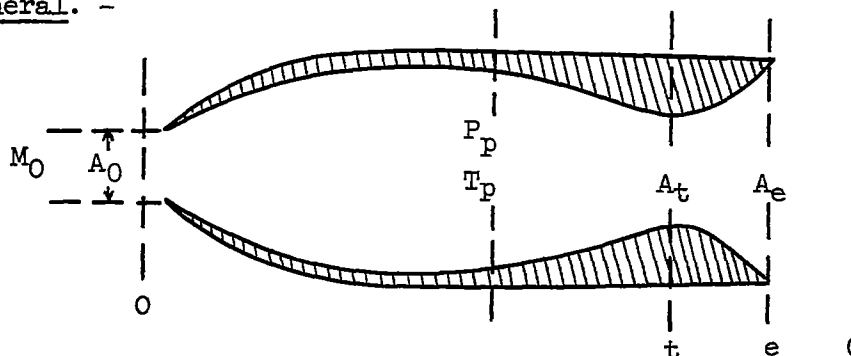
From momentum considerations, the net internal thrust for this configuration can be written:

$$F = p_e A_e (1 + \gamma M_e^2) - p_0 A_0 (1 + \gamma M_0^2) + p_0 (A_0 - A_e)$$

$$= p_e A_e (1 + \gamma M_e^2) - p_0 A_0 \gamma M_0^2 - p_0 A_e \tag{C1}$$

This expression is made dimensionless through division by $A_t P_p$:

$$\frac{F}{A_t P_p} = \frac{A_e}{A_t} \frac{p_e}{P_p} (1 + \gamma M_e^2) - \frac{p_0}{P_p} \frac{A_0}{A_t} \gamma M_0^2 - \frac{p_0}{P_p} \frac{A_e}{A_t} \tag{C2}$$

Assuming isentropic expansion in the nozzle (such as for ideal nozzle and for underexpanded flow cases) and using the continuity relation between stations 0 and t:

$$\frac{F}{A_t P_p} = \left(\frac{2}{\gamma+1}\right)^{\frac{\gamma+1}{2(\gamma-1)}} \left[\frac{\left(\frac{P_p}{p_e}\right)^{\frac{\gamma+1}{2\gamma}} \left[\left(\frac{p_e}{P_p}\right) \left\{ 1 + \left(\frac{2\gamma}{\gamma-1}\right) \left[\left(\frac{P_p}{p_e}\right)^{\frac{\gamma-1}{\gamma}} - 1 \right] \right\} - \frac{p_0}{P_p} \right]}{\sqrt{\left(\frac{2}{\gamma-1}\right) \left[\left(\frac{P_p}{p_e}\right)^{\frac{\gamma-1}{\gamma}} - 1 \right]}} - \gamma M_0 \sqrt{\frac{t_0}{T_p}} \right] \tag{C3}$$

Ideal nozzle. - For the ideal nozzle $p_e = p_0$; equation (C3) then becomes

$$\frac{F_i}{A_t P_p} = \left(\frac{2}{\gamma+1}\right)^{\frac{\gamma+1}{2(\gamma-1)}} \left[\gamma \left(\frac{p_p}{p_0}\right)^{\frac{1-\gamma}{2\gamma}} \sqrt{\frac{2}{\gamma-1}\left[\left(\frac{p_p}{p_0}\right)^{\frac{\gamma-1}{\gamma}} - 1\right]} - \gamma M_0 \sqrt{\frac{t_0}{T_p}}\right] \quad (C4)$$

Ideal convergent nozzle (choked). - For a choked exit section,

$$\frac{p_p}{p_e} = \left(\frac{\gamma+1}{2}\right)^{\frac{\gamma}{\gamma-1}}$$

Substituting in equation (C3) gives

$$\frac{F_{c_i}}{A_t P_p} = \left[(1+\gamma)\left(\frac{2}{\gamma+1}\right)^{\frac{\gamma}{\gamma-1}}\right]\left[1 - \frac{\gamma M_0}{\sqrt{2(\gamma+1)}}\sqrt{\frac{t_0}{T_p}}\right] - \frac{p_0}{p_p} \quad (C5)$$

2728

APPENDIX D

ASSUMPTIONS AND METHOD OF TURBOJET AND RAM-JET SAMPLE

CALCULATIONS FOR PRESSURE AND FORCE DATA

Turbojet Flight Plan and Assumptions

The schedule of engine pressure ratio r_e and inlet recovery r_i for the assumed turbojet flight plan is tabulated below:

M_0	r_e	r_i	Altitude	T_p
0.2	1.912	0.96	Sea	
.6	1.819	.96	level	
.9	1.715	.96	$t_0 = 519^\circ$ R	
0.9	2.115	0.96		3200° R
1.2	1.966	.94		
1.6	1.732	.90	Tropo-	
			pause	
1.9	1.545	.86		
2.3	1.289	.81	$t_0 = 392^\circ$ R	
2.7	1.180	.78		
3.0	1.989	.71		

The value of $\dfrac{F_{c_i}}{A_t P_p}$ is calculated from equation (C5) with

$$\frac{P_0}{P_p} = \frac{P_0}{P_0} \times \frac{1}{r_e r_i} = \frac{1}{r_e r_i \left(1 + \frac{\gamma-1}{2} M_0^2\right)^{\frac{\gamma}{\gamma-1}}} \tag{D1}$$

Ram-Jet Flight Plan and Assumptions

For the ram jet all flight is assumed at the tropopause with $M_0 \geq 0.9$. Inlet recovery is the same as for the turbojet in the tropopause and r_e is taken as 0.90. As before, $T_p = 3200^\circ$ R.

$$\frac{P_0}{P_p} = \frac{1}{0.9\, r_i \left(1 + \frac{\gamma-1}{2} M_0^2\right)^{\frac{\gamma}{\gamma-1}}} \tag{D2}$$

2728

Calculations of Incremental Thrust Ratio

Zero bleed momentum. - The incremental thrust ratio as calculated by use of the wall pressure data is

$$\frac{F - F_c}{F_{c_i}} = \frac{\int_1^{\frac{A_e}{A_t}} \left(\frac{p_w - p_0}{p_p}\right) d\left(\frac{A}{A_t}\right)}{\frac{F_{c_i}}{A_t p_p}} \tag{D3}$$

and by use of the force data is

$$\frac{F - F_c}{F_{c_i}} = \frac{\left(\frac{F_j}{\delta_t}\right)_a - \left(\frac{F_{j_c}}{\delta_t}\right)_a}{P_{sl} A_t \left(\frac{p_p}{p_0}\right)\left(\frac{F_{c_i}}{A_t p_p}\right)} \tag{D4}$$

External bleed. - The incremental thrust ratio as calculated by use of the wall pressure data is

$$\frac{F - F_c}{F_{c_i}} = \frac{\int_1^{\frac{A_e}{A_t}} \left(\frac{p_w - p_0}{p_p}\right) d\left(\frac{A}{A_t}\right) - \int_{A_s} \frac{\rho u^2}{p_p A_t} d(A_s)}{\frac{F_{c_i}}{p_p A_t}} \tag{D5}$$

When it is assumed that all the external bleed is from the free stream,

$$\int_{A_s} \frac{\rho u^2}{p_p A_t} d(A_s) = \gamma M_0^2 \left(\frac{p_0}{p_p}\right)\left(\frac{A_s}{A_t}\right)$$

From mass flow considerations,

$$A_s = \frac{W_s}{W_p} A_0 C_D = \left[\frac{W_s}{W_p} \sqrt{\frac{T_s}{T_p}}\right] \sqrt{\frac{T_p}{T_s}} A_0 C_D$$

2728

$$\int_{A_s} \frac{\rho u^2}{P_p A_t} \, dA_s = \frac{\gamma M_0 C_D}{\sqrt{1 + \frac{\gamma-1}{2} M_0^2}} \left(\frac{2}{\gamma+1}\right)^{\frac{\gamma+1}{2(\gamma-1)}} \left[\frac{W_s}{W_p} \sqrt{\frac{T_s}{T_p}}\right] \sqrt{\frac{T_0}{T_s}}$$

therefore

$$\frac{F - F_c}{F_{c_i}} = \frac{\displaystyle\int_1^{\frac{A_e}{A_t}} \left(\frac{p_w - p_0}{P_p}\right) d\left(\frac{A}{A_t}\right) - \frac{\gamma M_0 C_D}{\sqrt{1 + \frac{\gamma-1}{2} M_0^2}} \left(\frac{2}{\gamma+1}\right)^{\frac{\gamma+1}{2(\gamma-1)}} \left[\frac{W_s}{W_p} \sqrt{\frac{T_s}{T_p}}\right] \sqrt{\frac{T_0}{T_s}}}{\dfrac{F_{c_i}}{A_t P_p}}$$

(D5a)

In the above calculation, $\frac{W_s}{W_p} \sqrt{\frac{T_s}{T_p}}$ is chosen for the operating pressure ratio and value of $\frac{P_s}{P_p} = \left(\frac{P_s}{P_0}\right)\left(\frac{P_0}{P_p}\right)$ where $\frac{P_s}{P_0}$ is normal shock recovery at the flight Mach number (see, for instance, fig. 16). T_s was assumed equal to T_0.

The incremental thrust ratio as calculated by use of the force data is

$$\frac{F - F_c}{F_{c_i}} = \frac{\left(\frac{F_j}{\delta_t}\right)_a - P_{sl} A_t \left(\frac{P_p}{P_0}\right) \frac{\gamma M_0 C_D}{\sqrt{1 + \frac{\gamma-1}{2} M_0^2}} \left(\frac{2}{\gamma+1}\right)^{\frac{\gamma+1}{2(\gamma-1)}} \left[\frac{W_s}{W_p} \sqrt{\frac{T_s}{T_p}}\right] - \left(\frac{F_j}{\delta_t}\right)_{c_a}}{P_{sl} A_t \left(\frac{P_p}{P_0}\right)\left(\frac{F_{c_i}}{A_t P_p}\right)}$$

(D6)

REFERENCES

1. Tucker, Maurice: Approximate Calculation of Turbulent Boundary-Layer Development in Compressible Flow. NACA TN 2337, 1951.

2. Donaldson, Coleman duP., and Lange, Roy H.: Study of the Pressure Rise Across Shock Waves Required to Separate Laminar and Turbulent Boundary Layers. NACA TN 2770, 1952. (Supersedes NACA RM L52C21.)

3. Krull, H. George, and Steffen, Fred W.: Performance Characteristics of One Convergent and Three Convergent-Divergent Nozzles. NACA RM E52H12, 1952.

TABLE I. - NOZZLE COORDINATES

x (in.)	y_corr (in.)	y (in.)
-5.00		2.50
-3.00	2.33	2.39
-2.00	2.20	2.24
-1.28	2.10	2.132
- .70	2.04	2.063
- .35	2.01	2.029
0	2.000	2.015
.932	2.043	2.054
1.044	2.054	2.065
1.171	2.070	2.080
1.317	2.090	2.100
1.486	2.116	2.126
1.683	2.148	2.158
1.911	2.182	2.191
2.484	2.269	2.279
3.139	2.365	2.377
3.907	2.467	2.480
4.338	2.519	2.534
4.809	2.569	2.586
5.310	2.618	2.636
5.882	2.665	2.685
6.496	2.711	2.733
7.159	2.749	2.773
7.937	2.783	2.808
8.895	2.803	2.830
10.400	2.815	2.844

TABLE II. - WALL STATIC-TAP LOCATIONS

Tap	x (in.)	Orientation α (deg) (fig. 2)
1	0	0
2	.75	0
3	1.25	0
4	1.50	0
5	1.75	0
6	2.00	0
7	2.25	0
8	2.50	0
9	2.75	0
10	3.25	0
11	3.25	45
12	3.25	90
13	3.25	135
14	3.25	180
15	3.25	225
16	3.25	270
17	3.25	315
18	4.25	0
19	5.25	0
20	6.50	0
21	8.00	0
22	9.50	0
23	9.50	45
24	9.50	90
25	9.50	135
26	9.50	180
27	9.50	225
28	9.50	270
29	9.50	315

2728

NACA

2728
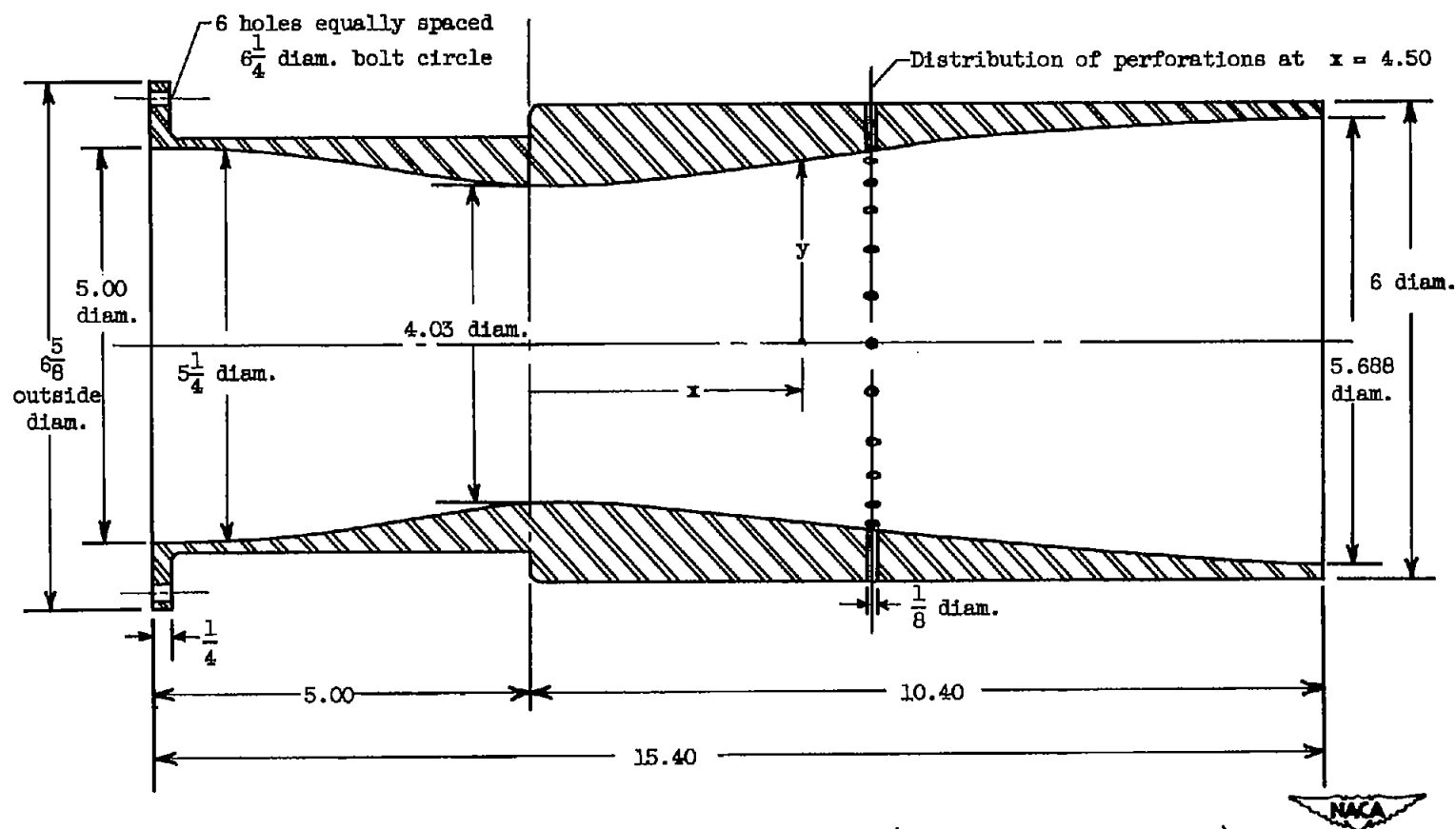
Figure 1. - Basic nozzle used in this investigation.   (Dimensions are in inches.)
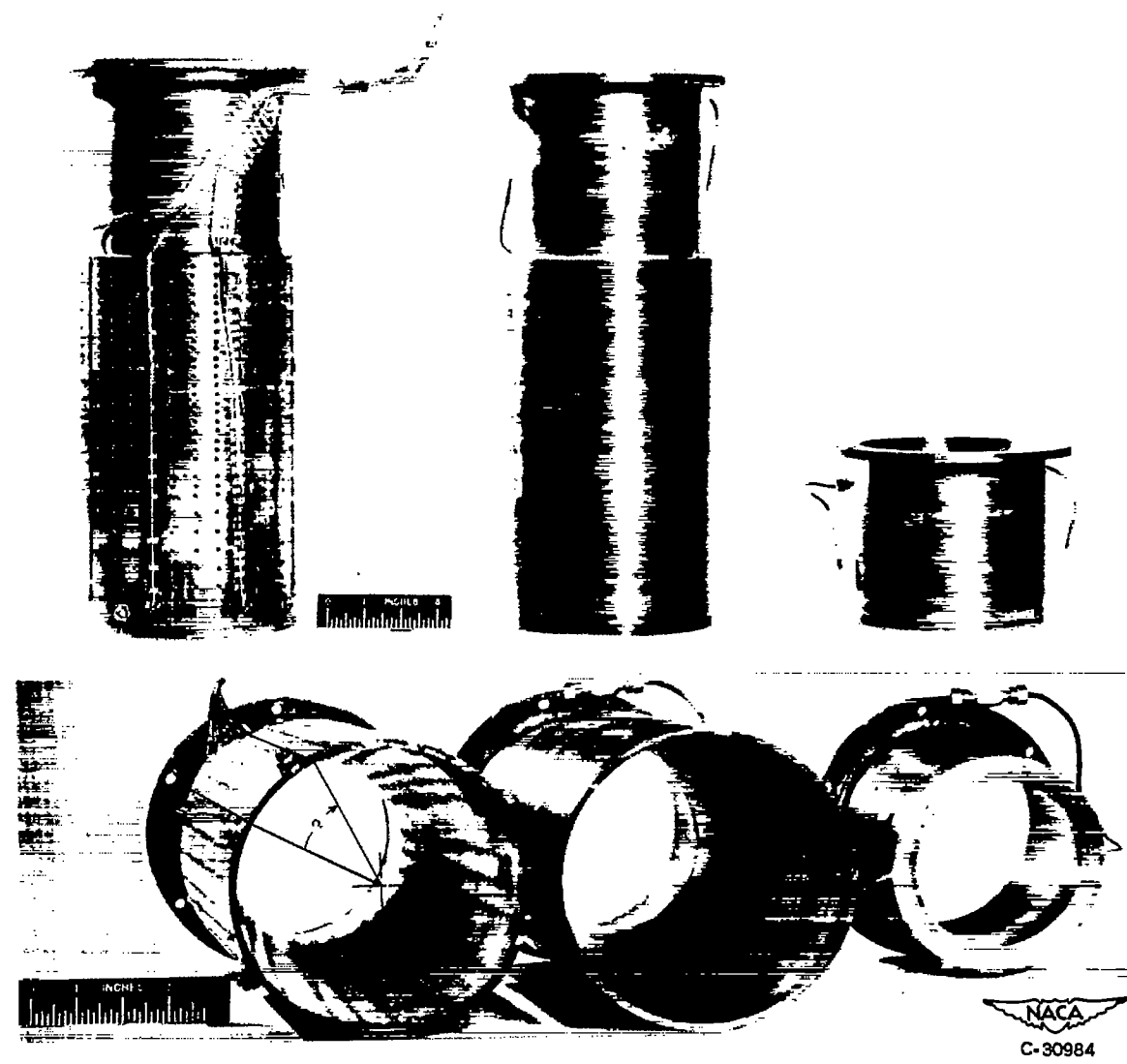
Perforated convergent-   Unperforated convergent-   Convergent nozzle
divergent nozzle   divergent nozzle

C-30984

Figure 2. - Photographs of nozzles investigated.

CONFIDENTIAL

2712

Air intake
from room

Inlet total-
pressure tap

P_p

To manometer
board

Static-pressure
tubes

P_s

A_t

Nozzle

Plate A
without holes

Plate A
with holes

A_e

P_0

Exhauster line

NACA
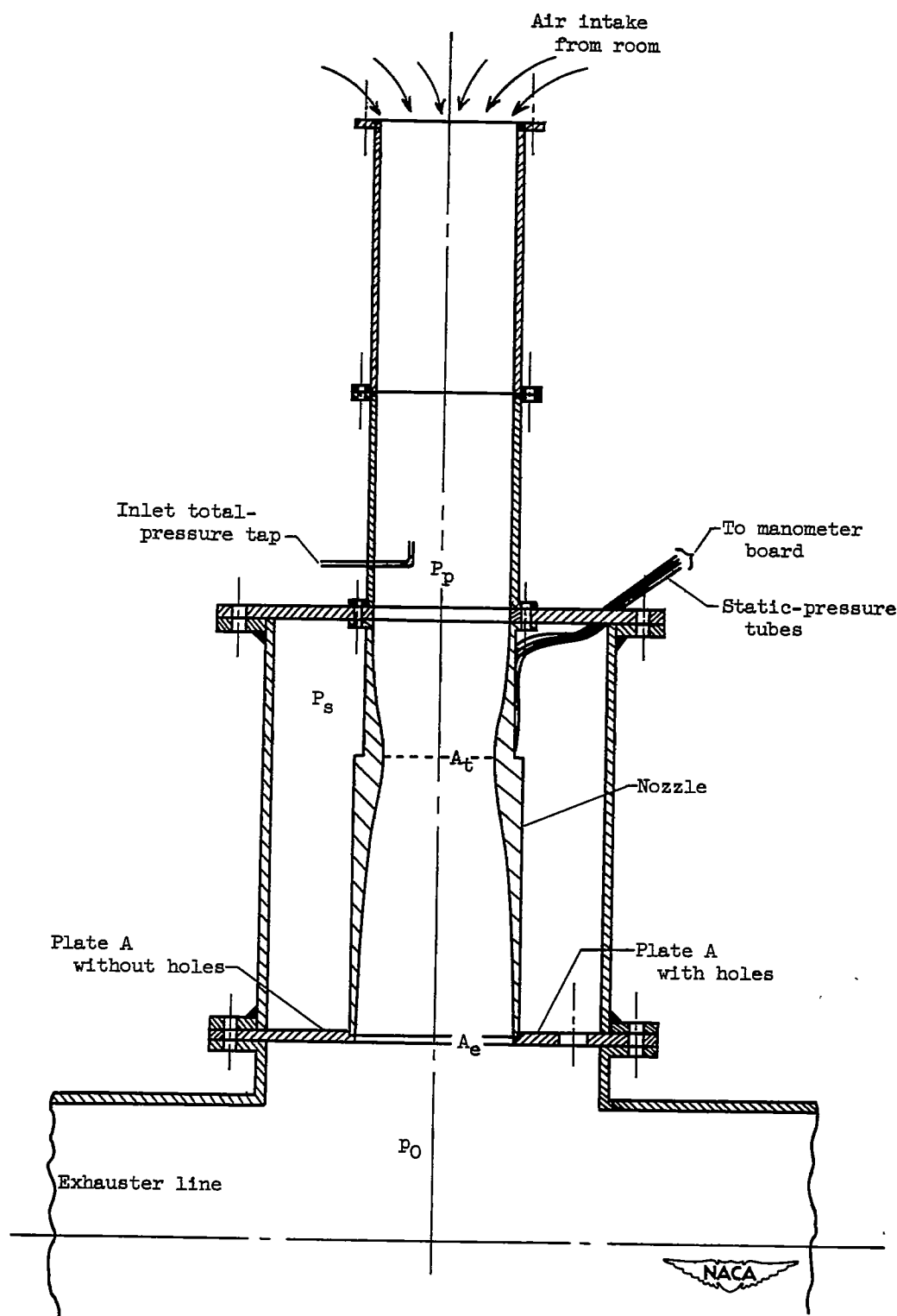
Figure 3. - Setup at duct station.

CONFIDENTIAL

2728
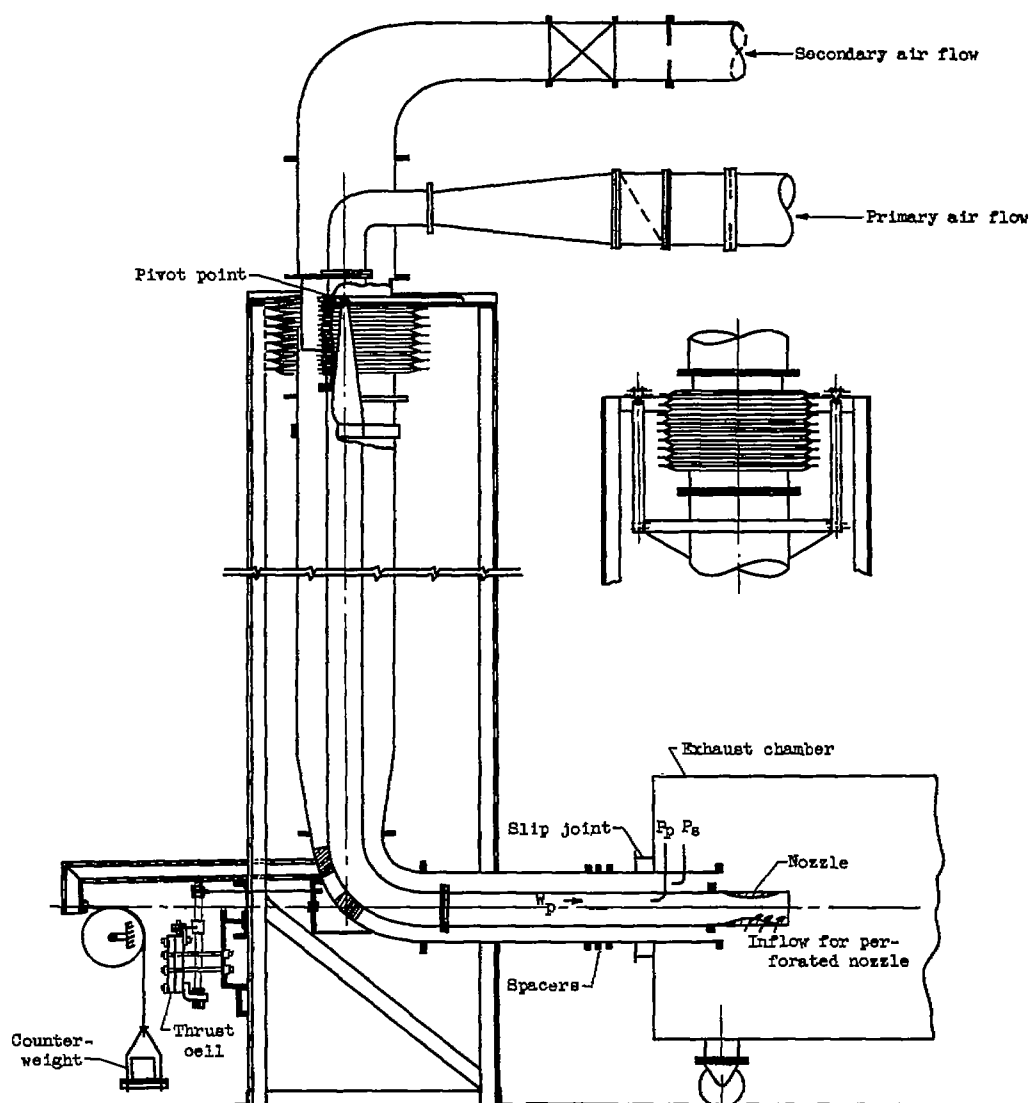
(a) Thrust rig details and setup for unperforated nozzle and for unshrouded perforated nozzle with ambient inbleed.
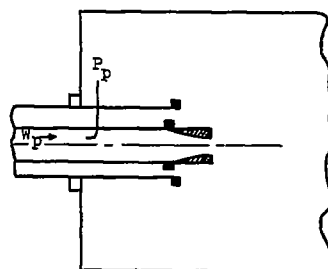
(b) Convergent nozzle.
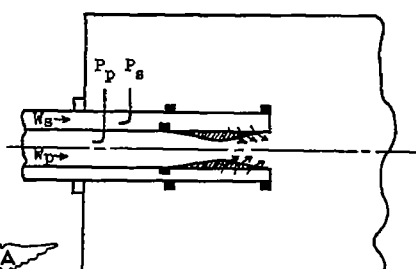
(c) Shrouded perforated nozzle with bleed.

Figure 4. - Setups at thrust rig.
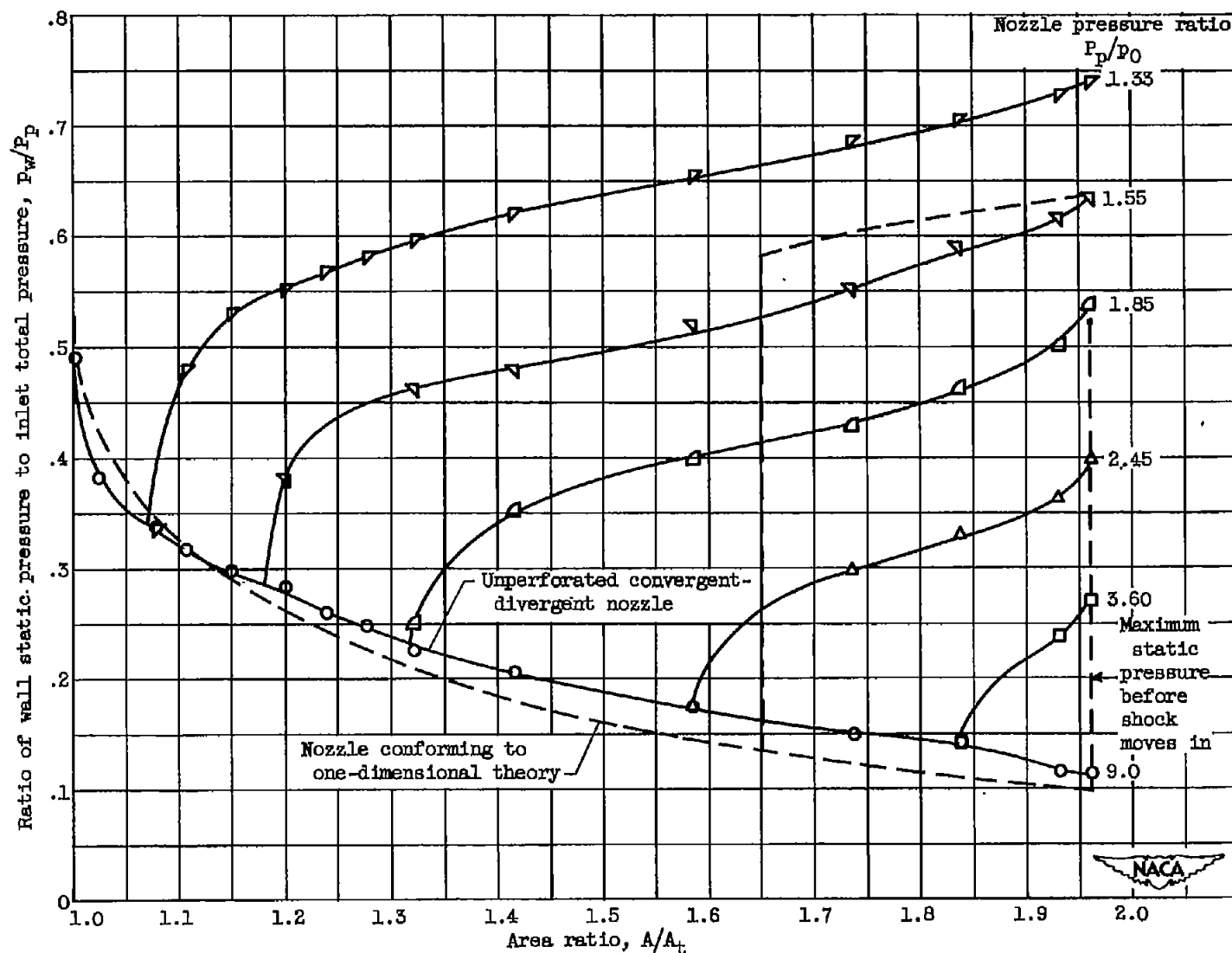
Figure 5. - Wall static-pressure distribution in divergent portion of unperforated convergent-divergent nozzle for various nozzle pressure ratios.
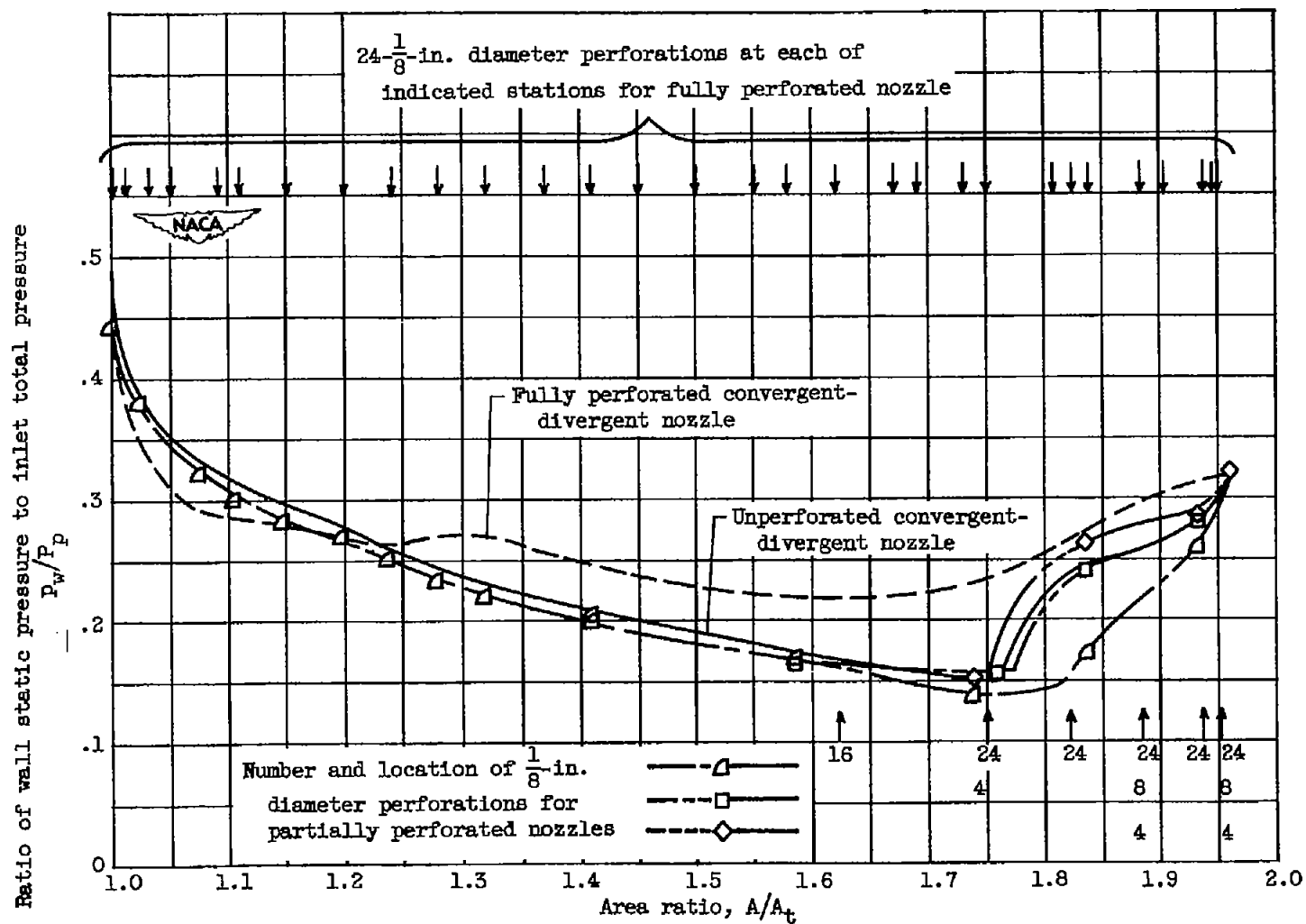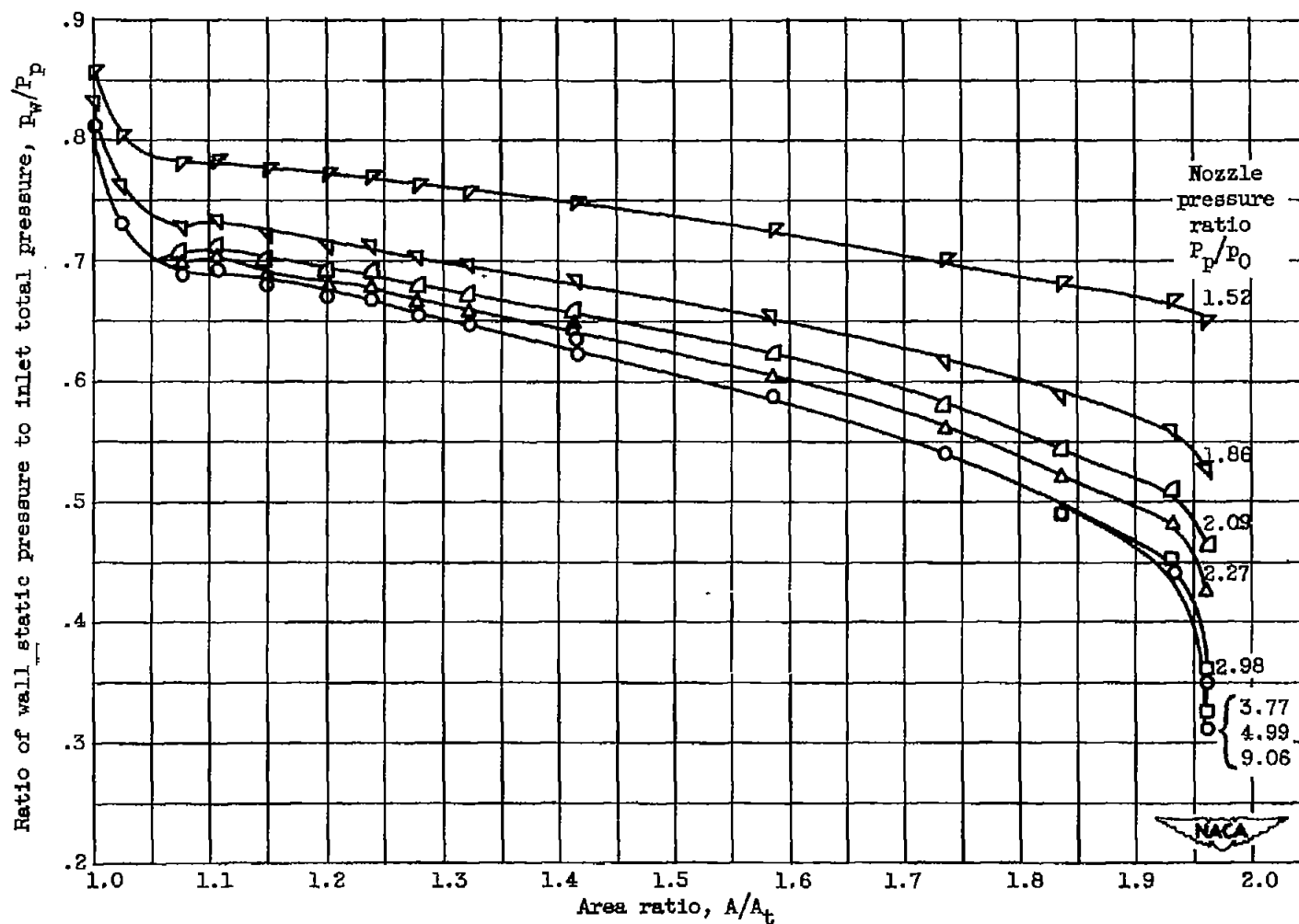
(a) Nozzle pressure ratio, 3.0.

Figure 6. - Wall static-pressure distribution with various numbers of perforations and ambient bleed.

2728
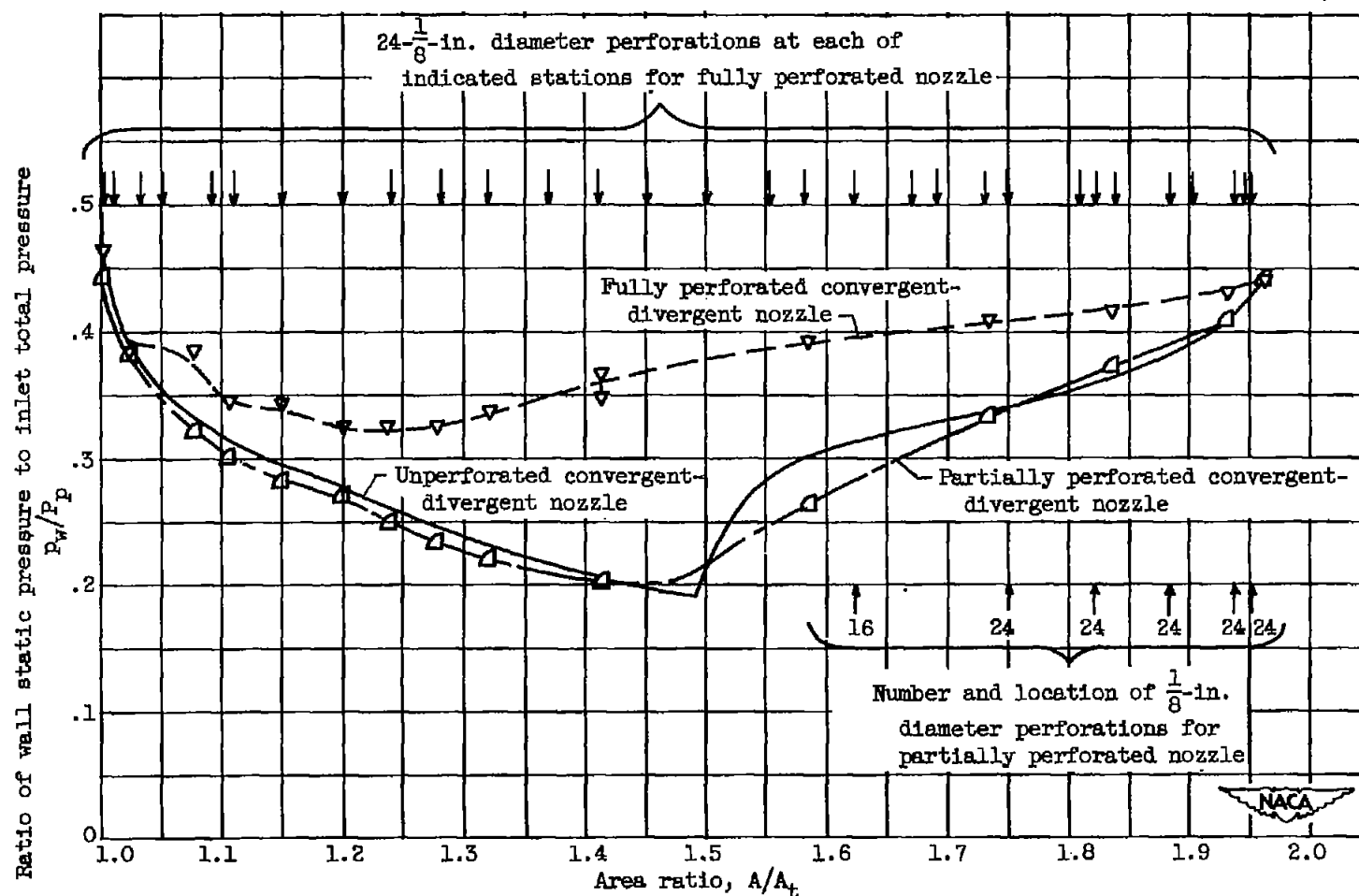
(b) Nozzle pressure ratio, 2.2.

Figure 6. - Concluded. Wall static-pressure distribution with various numbers of
perforations and ambient bleed.
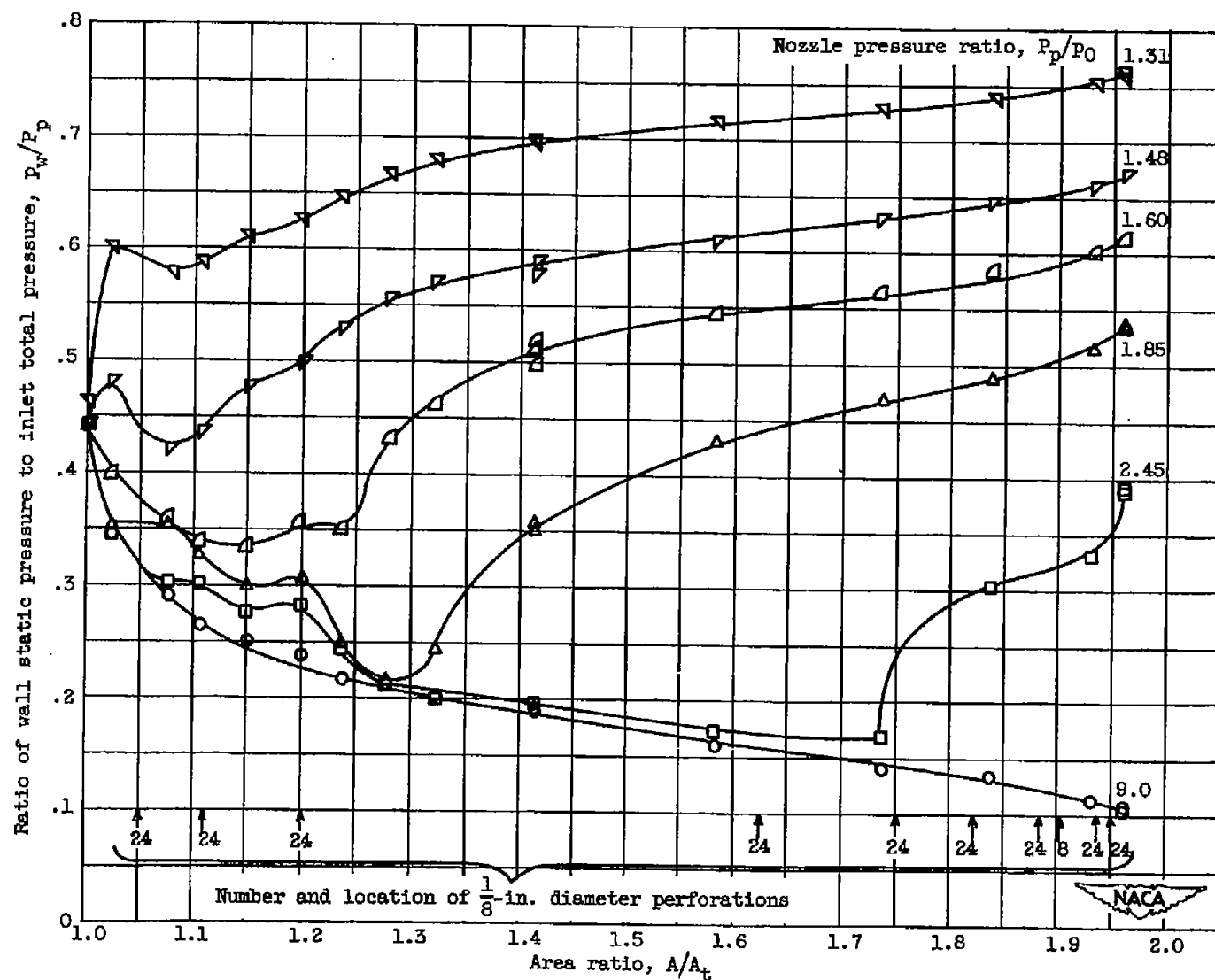
Figure 7. - Effect of local concentration of perforations on wall static-pressure distribution with ambient bleed.
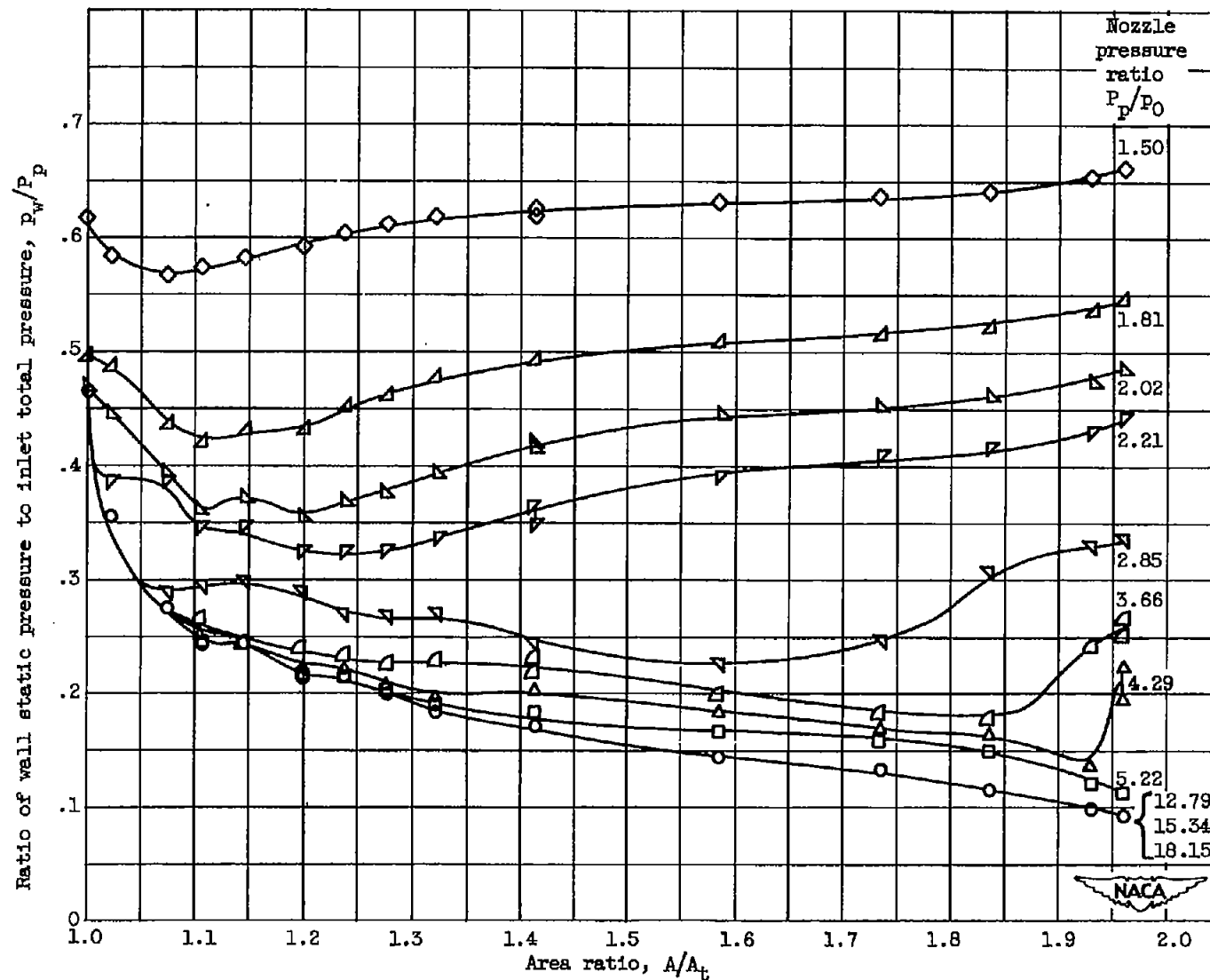
Figure 8. - Wall static-pressure distribution in divergent portion of perforated convergent-divergent nozzle with ambient bleed for various nozzle pressure ratios.
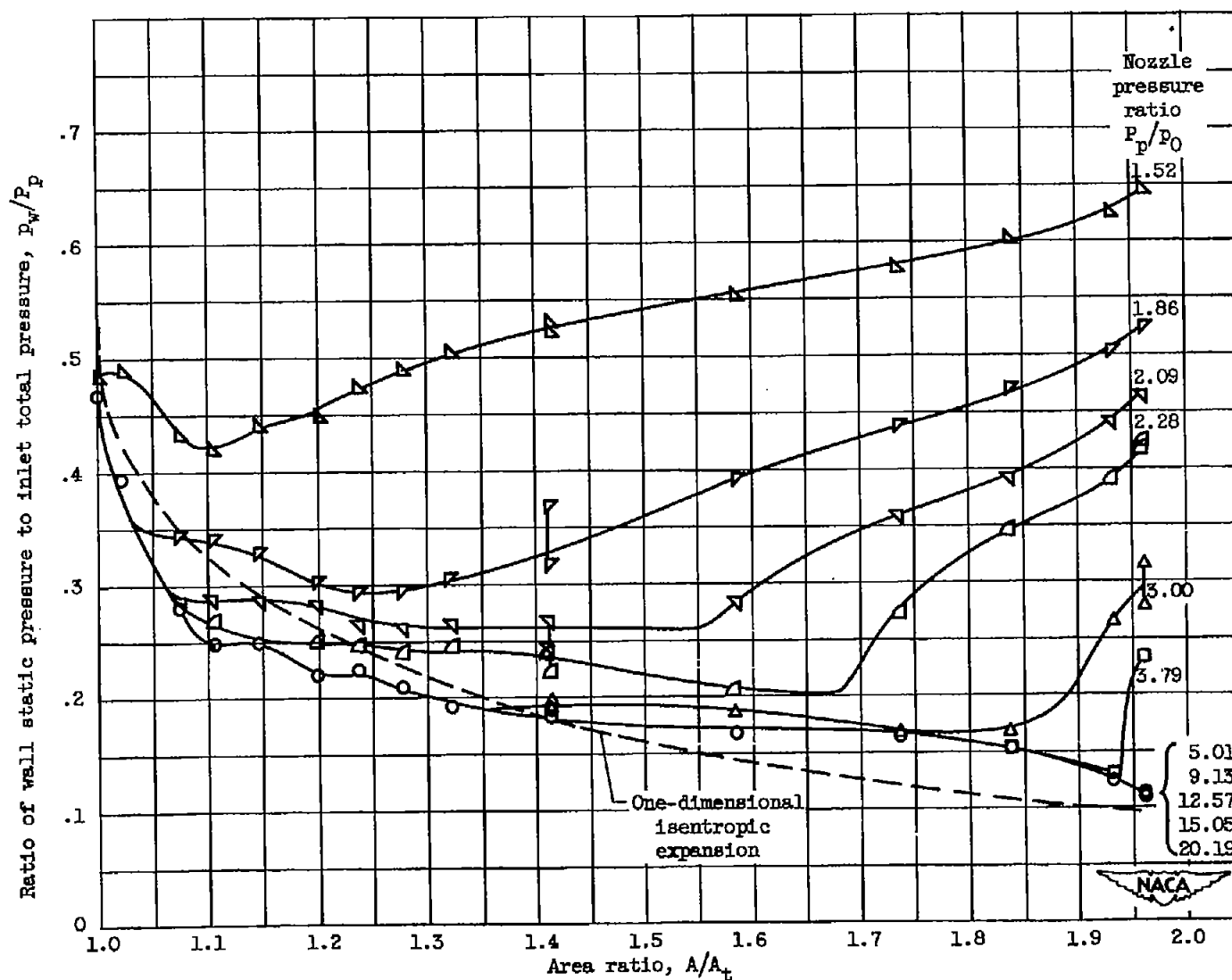
Figure 9. - Wall static-pressure distribution in divergent portion of shrouded perforated convergent-divergent nozzle with no bleed for various nozzle pressure ratios.

NACA RM E52J27

2728
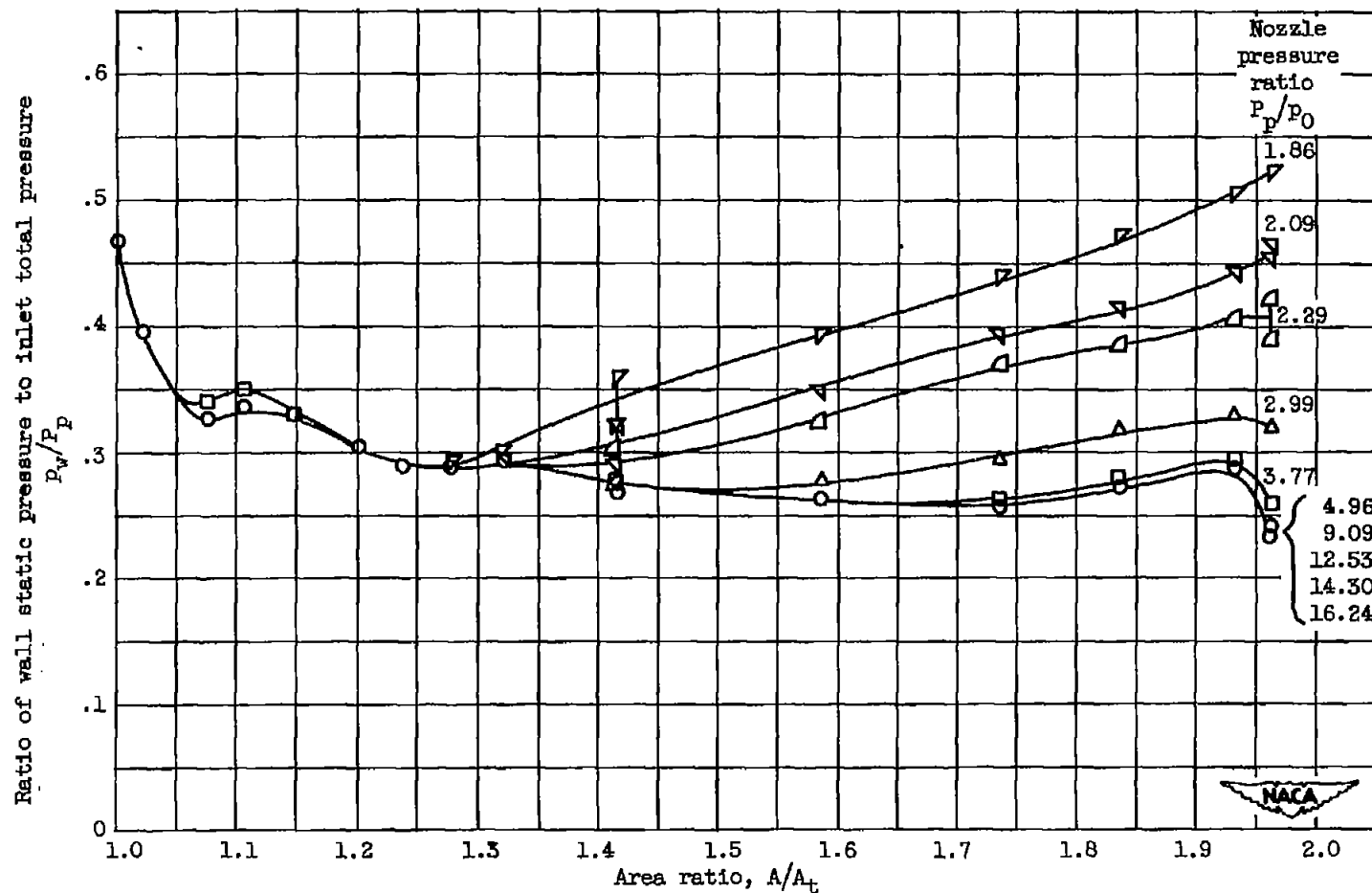
(a) Ratio of bleed total pressure to inlet total pressure, 0.4.

Figure 10. - Wall static-pressure distribution in divergent portion of shrouded perforated convergent-divergent nozzle with bleed at various nozzle pressure ratios and bleed pressure ratios.

(b) Ratio of bleed total pressure to inlet total pressure, 1.0.

Figure 10. - Concluded. Wall static-pressure distribution in divergent portion of shrouded perforated convergent-divergent nozzle with bleed at various nozzle pressure ratios and bleed pressure ratios.

2728
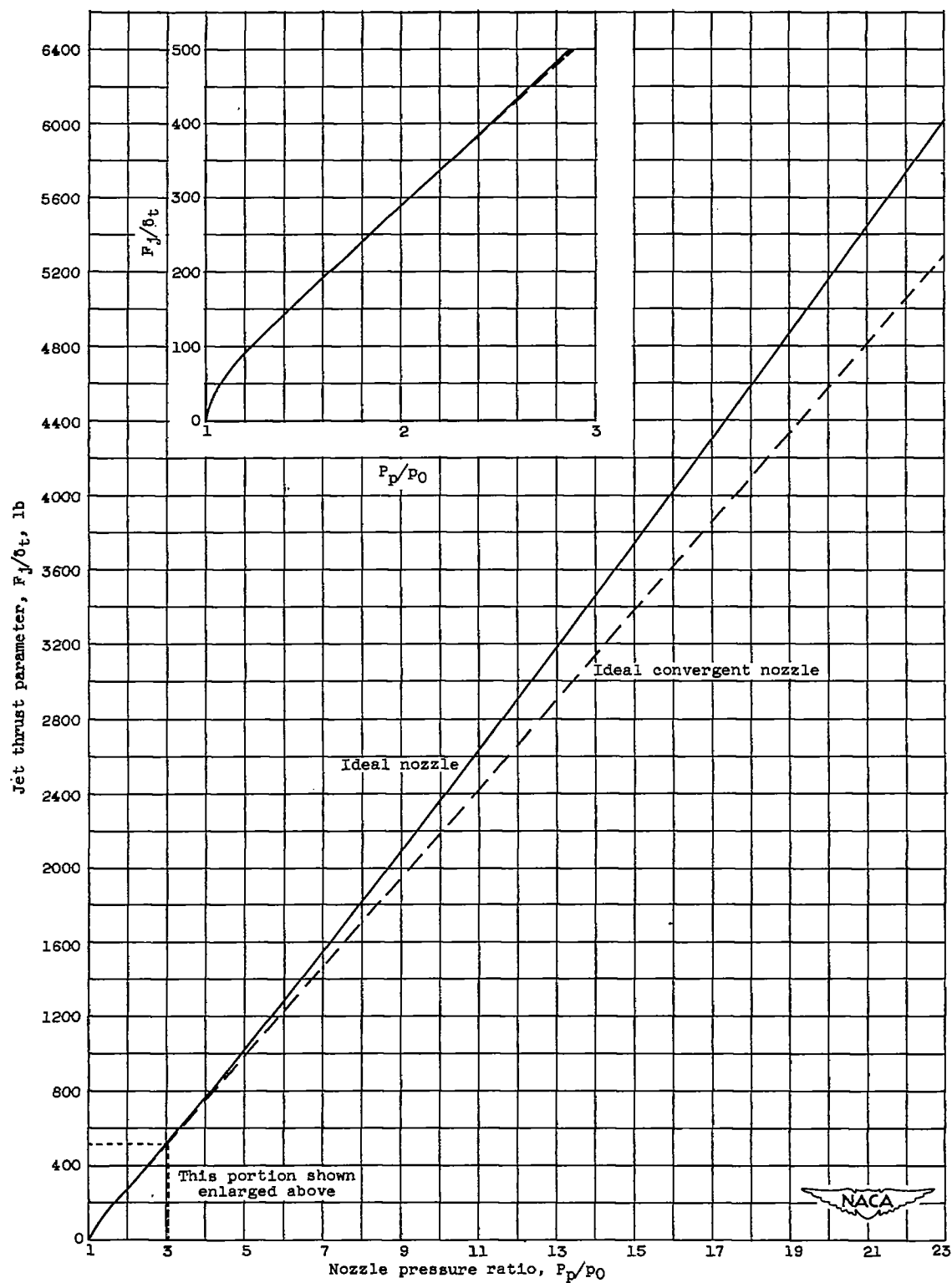
Figure 11. - Jet thrust of ideal nozzle and of ideal convergent nozzle.
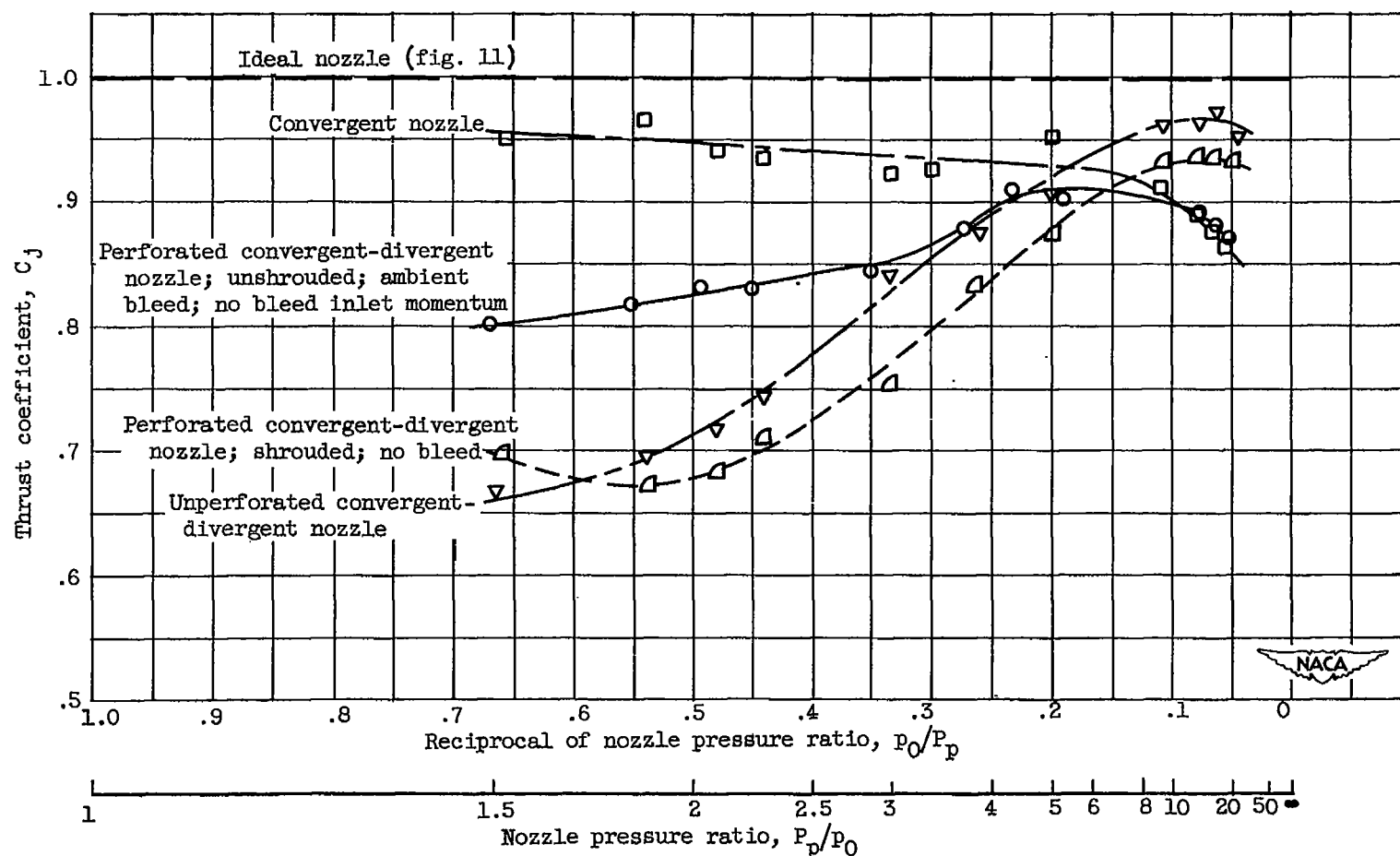
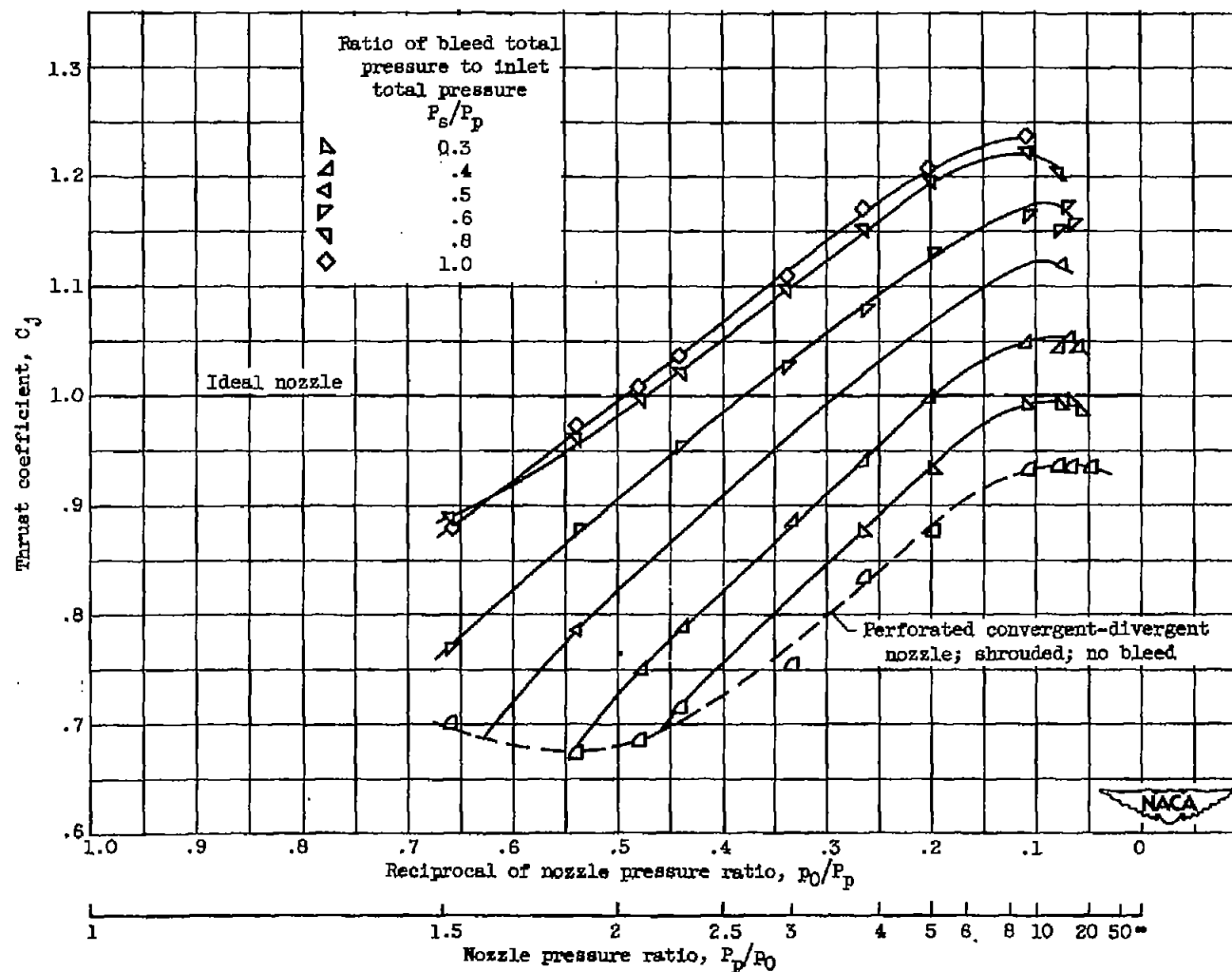Figure 12. - Thrust coefficient variation with nozzle pressure ratio.

2728

(a) Comparison for constant total mass flow.

Figure 13. - Variation of thrust coefficient with nozzle pressure ratio for pressurized bleed through perforations.

36

CONFIDENTIAL

NACA RM E52J27

(b) Comparison for constant throat area.

Figure 13. - Concluded. Variation of thrust coefficient with nozzle pressure ratio for pressurized bleed through perforations.
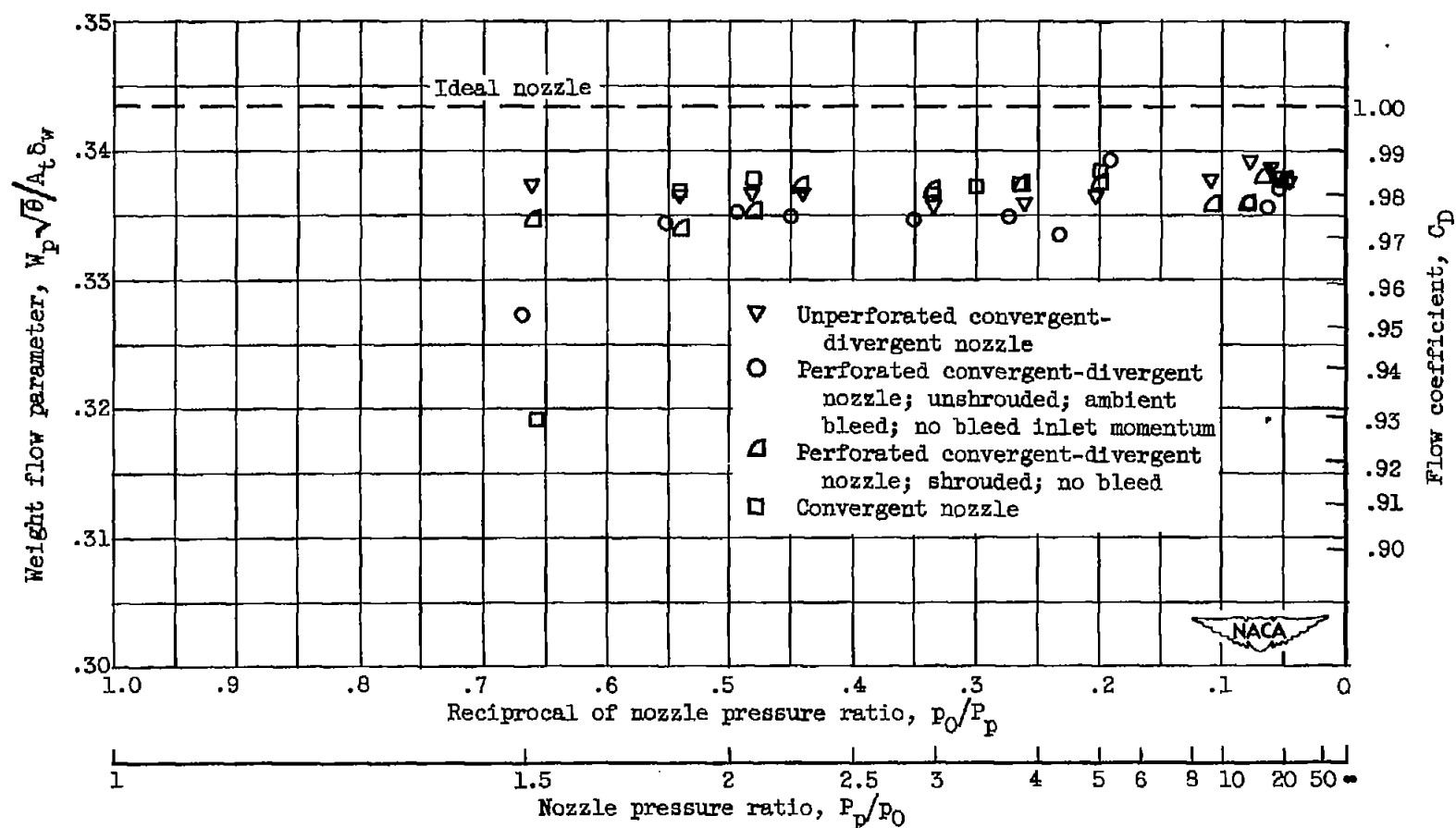
2728

.35

Ideal nozzle

.34

Weight flow parameter, $W_p \sqrt{\theta}/A_t \delta_w$

.33

TUNNEL DOWNS

.32

.31

.30

1.0   .9   .8   .7   .6   .5   .4   .3   .2   .1   0

Reciprocal of nozzle pressure ratio, p_0/P_p

1   1.5   2   2.5   3   4   5   6   8   10   20   50   ∞

Nozzle pressure ratio, P_p/p_0

1.00
.99
.98
.97
.96
.95
.94
.93
.92
.91
.90

Flow coefficient, C_D

∇   Unperforated convergent-
      divergent nozzle
O   Perforated convergent-divergent
      nozzle; unshrouded; ambient
      bleed; no bleed inlet momentum
◁   Perforated convergent-divergent
      nozzle; shrouded; no bleed
□   Convergent nozzle

NACA

CONFIDENTIAL

37

Figure 14. - Weight flow and flow coefficient variation with nozzle pressure ratio.
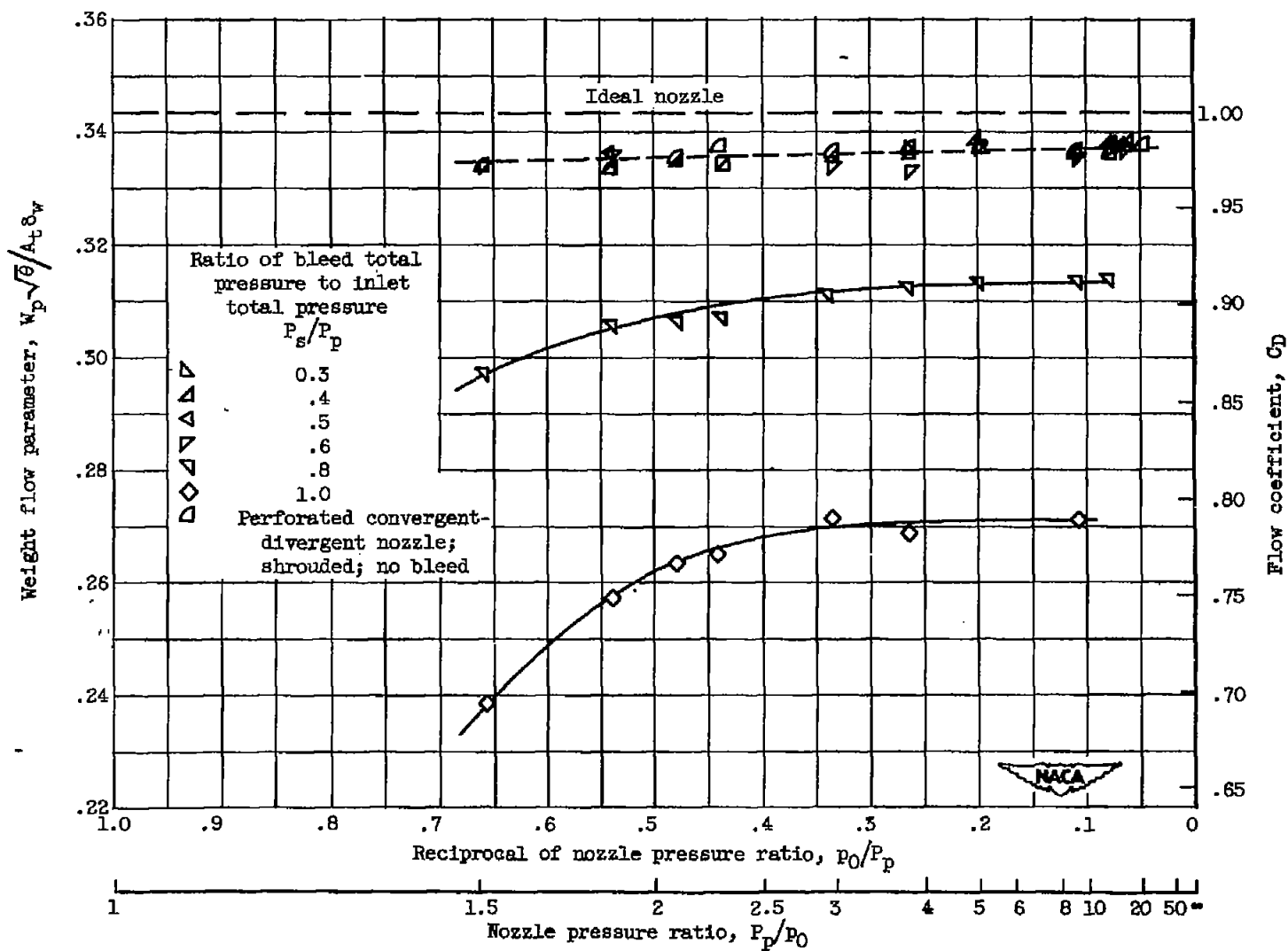
Figure 15. - Weight flow and flow coefficient variation with nozzle pressure ratio for pressurized bleed through perforations.
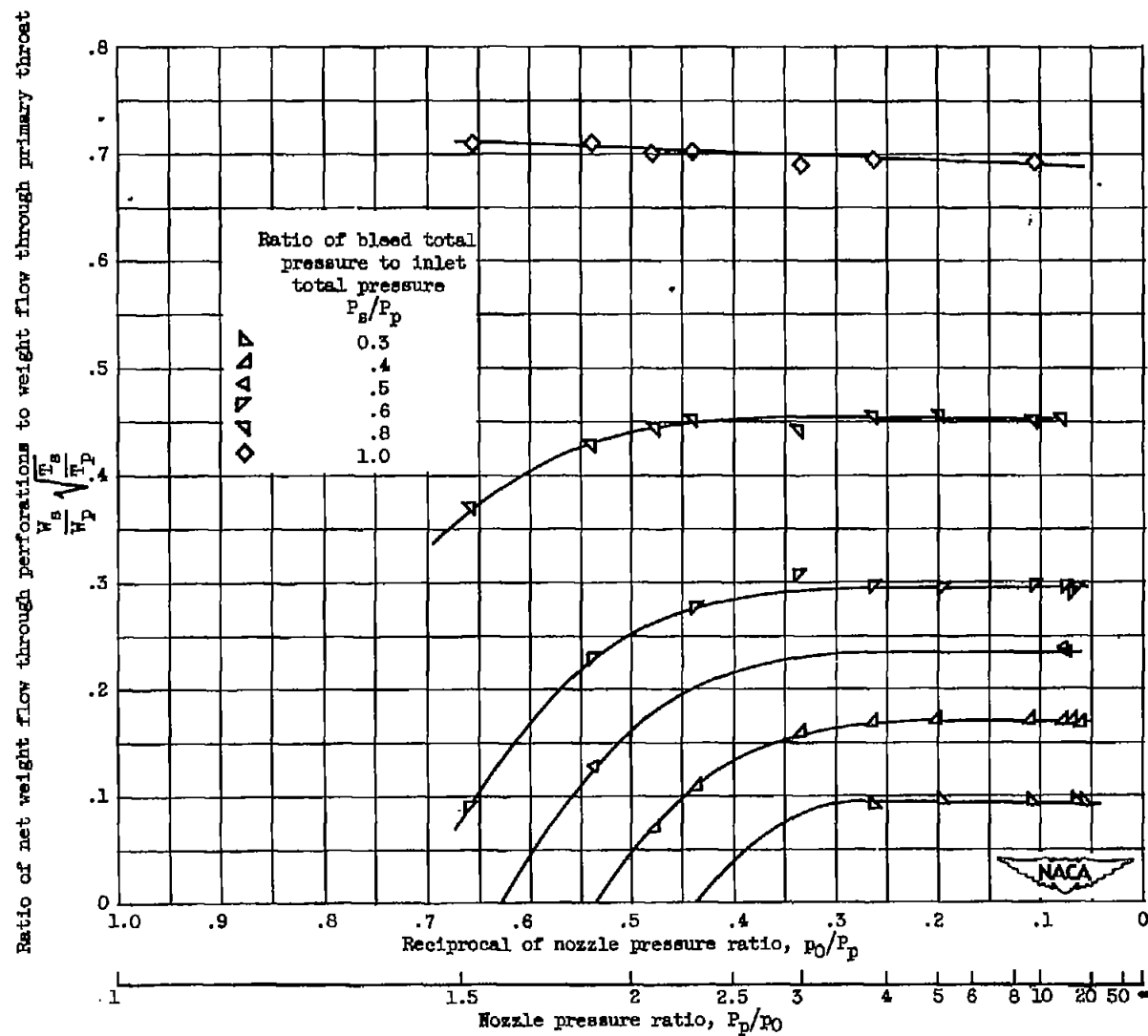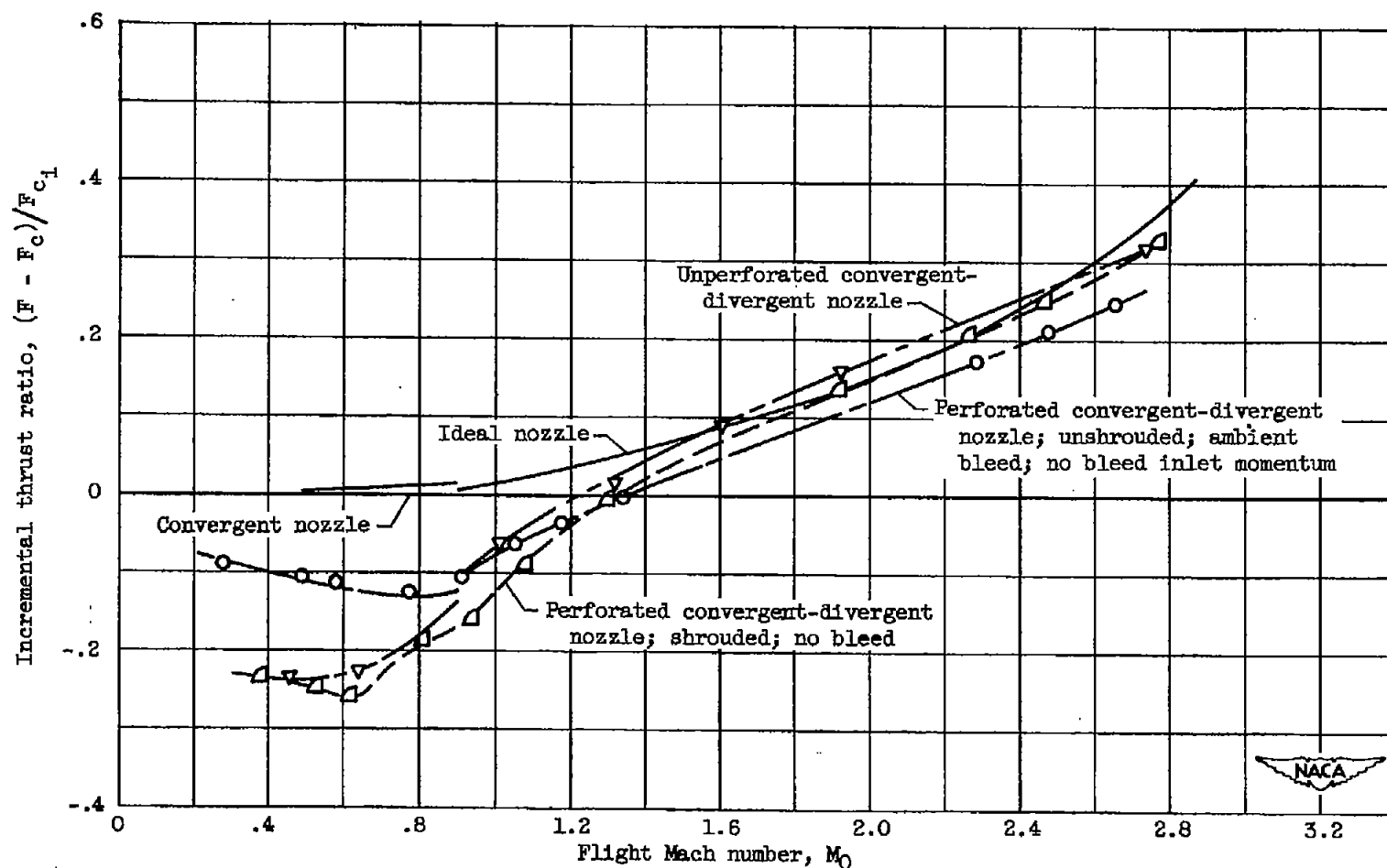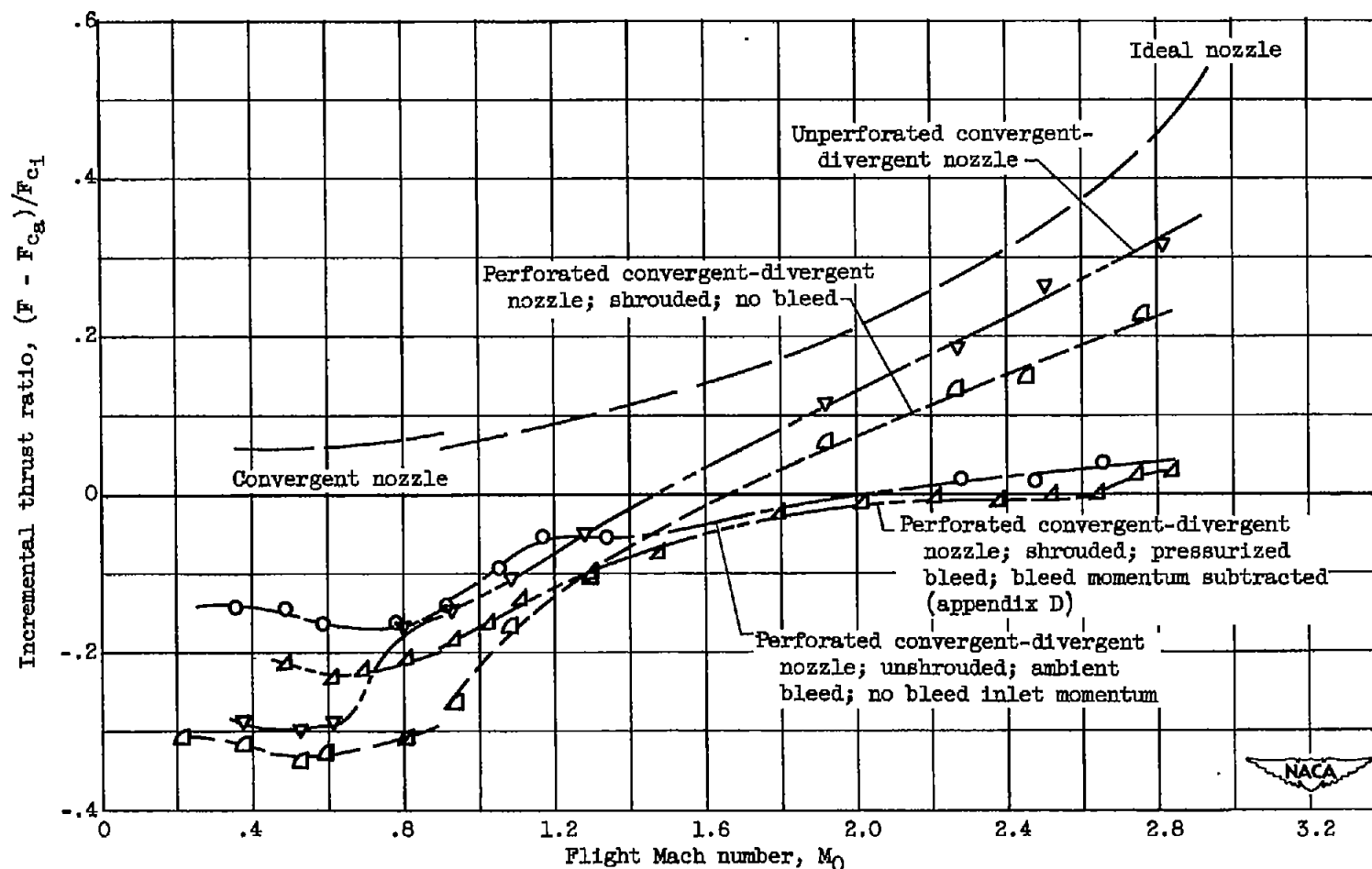
Figure 16. - Variation of net weight flow through perforations with bleed total pressure and nozzle pressure ratio.

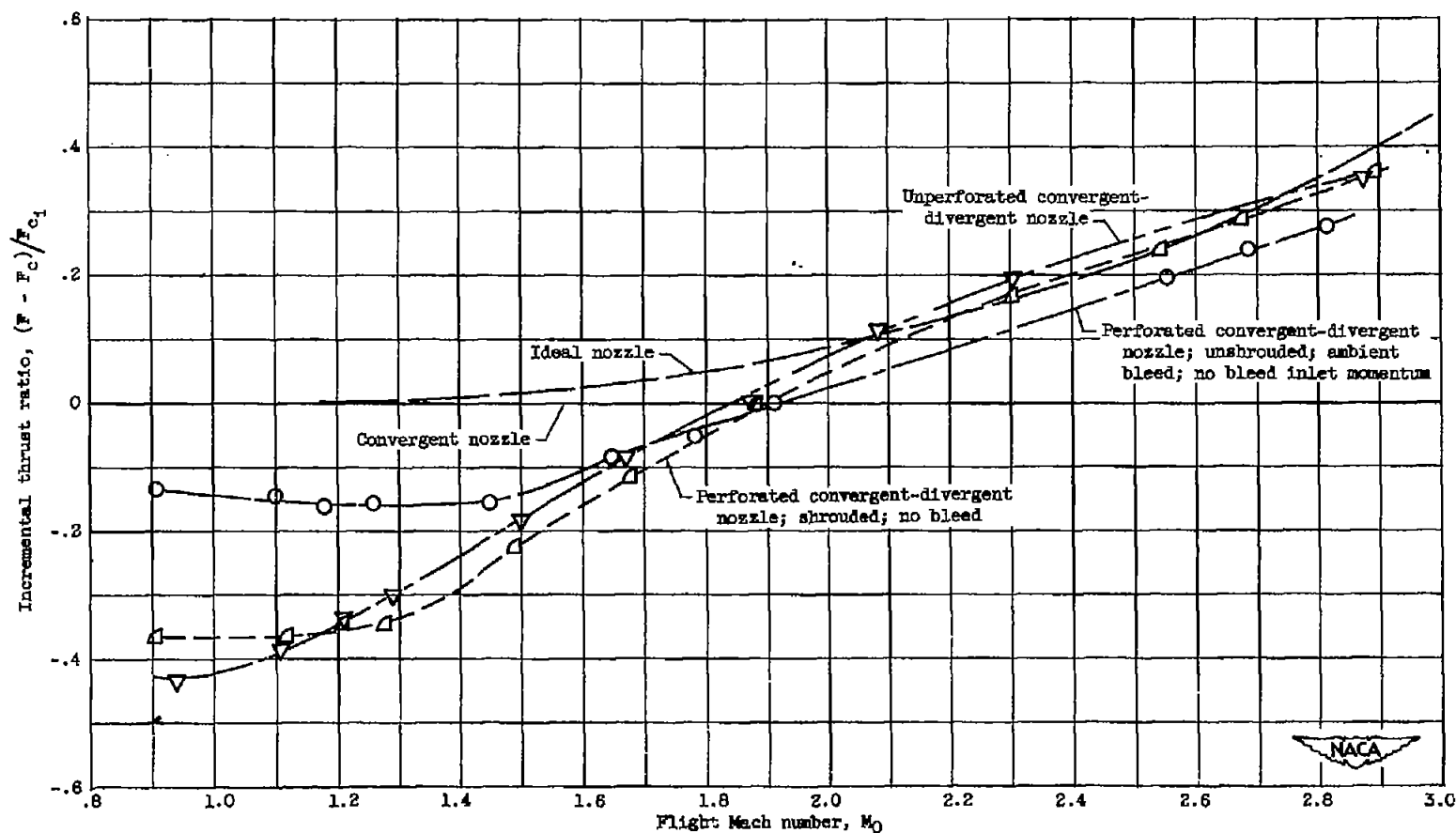(a) Data based on integration of wall static pressures.

Figure 17. - Variation of incremental thrust ratio with flight Mach number for various nozzle configurations; turbojet flight assumptions.

(b) Force data.

Figure 17. - Concluded. Variation of incremental thrust ratio with flight Mach number for various
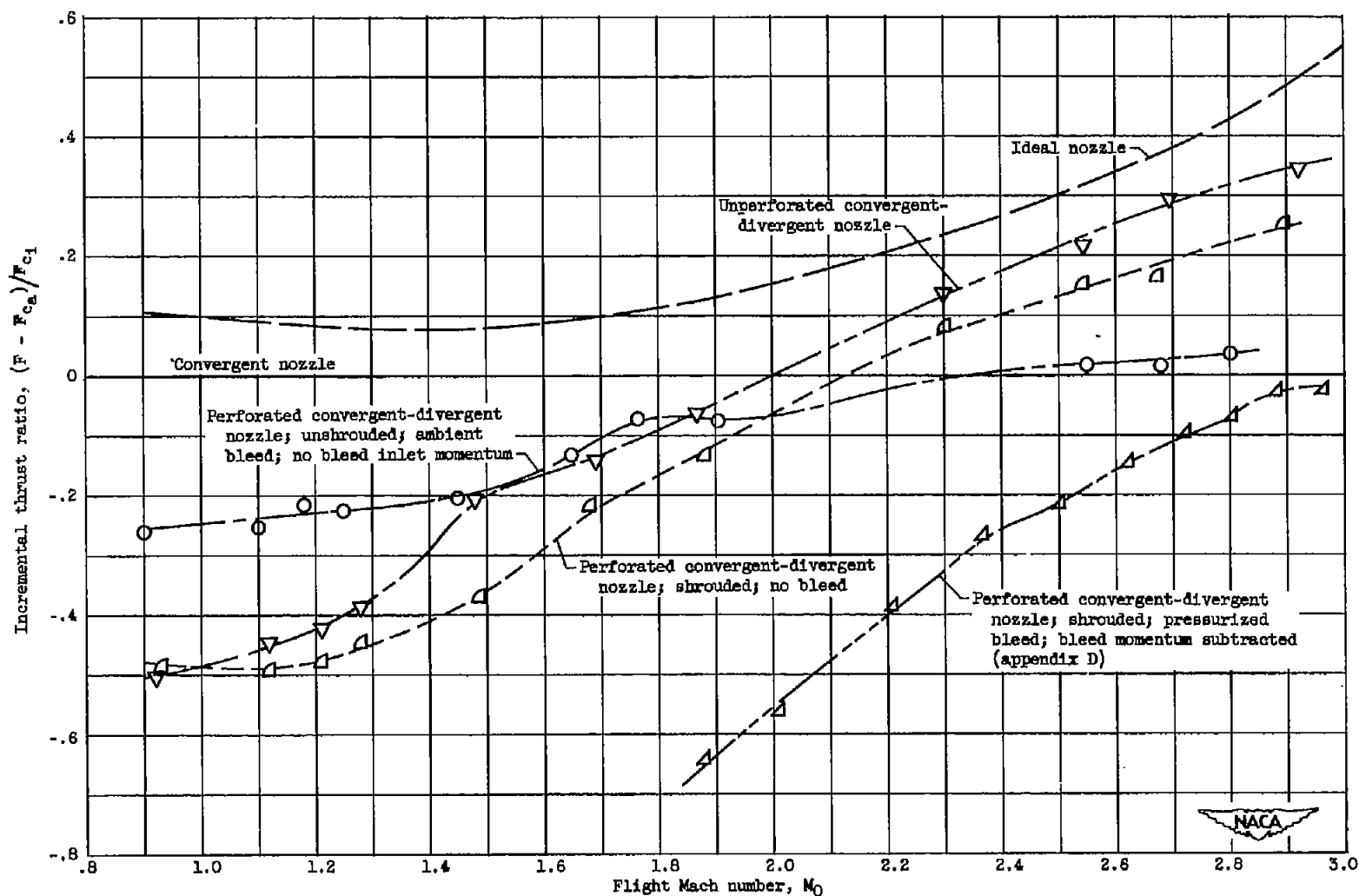nozzle configurations; turbojet flight assumptions.

(a) Data based on integration of wall static pressures.

Figure 18. - Variation of incremental thrust ratio with flight Mach number for various nozzle configurations; ram jet flight assumptions.

(b) Force data.

Figure 18. - Concluded. Variation of incremental thrust ratio with flight Mach number for various nozzle configurations; ram jet flight assumptions.